

Physics-aware Truck and Drone Delivery Planning Using Optimization & Machine Learning

Yineng Sun

Thayer School of Engineering, Dartmouth College, Hanover, NH, United States of America, yineng.sun.th@dartmouth.edu,

Armin Fügenschuh

Brandenburgische Technische Universität Cottbus-Senftenberg, Cottbus, Germany, fuegensc@b-tu.de,

Vikrant Vaze

Thayer School of Engineering, Dartmouth College, Hanover, NH, United States of America, vikrant.s.vaze@dartmouth.edu,
<https://engineering.dartmouth.edu/community/faculty/vikrant-vaze>

Combining an energy-efficient drone with a high-capacity truck for last-mile package delivery can benefit operators and customers by reducing delivery times and environmental impact. However, directly integrating drone flight dynamics into the combinatorially hard truck route planning problem is challenging. Simplified models that ignore drone flight physics can lead to suboptimal delivery plans. We propose an integrated formulation for the joint problem of truck route and drone trajectory planning and a new end-to-end solution approach that combines optimization and machine learning to generate high-quality solutions in practical online runtimes. Our solution method trains neural network predictors based on offline solutions to the drone trajectory optimization problem instances to approximate drone flight times, and uses these approximations to optimize the overall truck-and-drone delivery plan by augmenting an existing order-first-split-second heuristic. Our method explicitly incorporates key kinematics and energy equations in drone trajectory optimization, and thereby outperforms state-of-the-art benchmarks that ignore drone flight physics. Extensive experimentation using synthetic datasets and real-world case studies shows that the integration of drone trajectories into package delivery planning substantially improves system performance in terms of tour duration and drone energy consumption. Our modeling and computational framework can help delivery planners achieve annual savings worth millions of dollars while also benefiting the environment.

Key words: truck and drone logistics, unmanned aerial vehicles, vehicle routing, last-mile delivery, combinatorial optimization, machine learning, neural networks

History:

1. Introduction

Recent years have witnessed explosive growth of the e-commerce sector. E-commerce sales increased by 6.1% in Q1 of 2025 from Q1 of 2024, accounting for 16.2% of all sales (US Census Bureau 2025). Optimizing e-commerce delivery logistics has become increasingly crucial for improving profits and customer experience. Given the large number of packages to be delivered to customers in a timely and cost-effective manner, small but consistent improvements in delivery strategies can have a significant bottom-line impact.

Last-mile deliveries are typically performed by trucks, each operating in a predefined region within urban, suburban, or rural areas. Recent technological developments in unmanned aerial vehicles—also called drones—have led to new last-mile delivery schemes that pair trucks with drones to assist in package delivery. To describe the optimization problems in this setup, Murray and Chu (2015) coined the name, the flying sidekick traveling salesman problem (FSTSP). Since then, many studies have focused on different FSTSP variants, often using slightly different names and problem specifications. In particular, Agatz et al. (2018) defined and studied the traveling salesman problem with drones (TSP-D), where, for a single truck and a single drone, the delivery assignments and vehicle routes are optimized jointly. Unlike the arc-based modeling approach commonly used in FSTSP, TSP-D divides the entire truck-and-drone tour into segments called operations and uses binary variables to decide whether to select each operation to create the tour.

Package delivery optimization studies typically estimate drone travel times using simplified flight trajectory models. Recent advances in drone trajectory modeling capture some of the relevant flight physics to calculate travel times and drone energy consumption more accurately. Schmidt and Fügenschuh (2023) modeled drone flights to generate precise, realizable and efficient trajectories, flight times, and drone energy consumption. Incorporating physics-based modeling of drone trajectories within the TSP-D framework can lead to a joint model that is more accurate but also more complicated. Given the associated computational difficulty, it is not yet clear to what extent such an integration might provide practical benefits. This paper shows that the common simplifications of drone flight physics used in truck-and-drone delivery optimization studies produce operational plans that can be highly suboptimal, demonstrating the need for better integration of nonlinear drone trajectory models within the combinatorial truck-and-drone planning problem.

Truck-and-drone delivery planning is a hard combinatorial optimization problem on its own, even with simplified drone-physics assumptions. Therefore, direct incorporation of drone trajectory equations into the base truck-and-drone delivery planning model is computationally intractable for realistic-sized problem instances. This paper proposes a drone-physics-aware truck-and-drone delivery planning model and an end-to-end solution approach that combines optimization and supervised learning to generate high-quality solutions in limited computational time. Extensive computational experimentation confirms that our approach scales well to real-world problem instances and outperforms computational and practical benchmarks consistently and substantially. Moreover, our model also incorporates restricted airspace constraints and enables drone take-off and landing on a moving truck to facilitate additional energy savings while ensuring safety.

This paper makes three contributions. First, we propose an integrated model of truck-and-drone delivery planning that combines nonlinear drone-trajectory physics with the combinatorial complexity of truck-and-drone route planning. Second, we develop an end-to-end solution approach that solves the resulting large-scale optimization model, using a neural network predictor combined with an augmented order-first-split-second routing heuristic. Third, we implement our modeling and algorithmic framework through a series of real-world case studies to demonstrate its practicality, substantial benefits, and operational insights.

2. Related Literature

This paper integrates nonlinear nonconvex relationships that describe drone flight physics into a combinatorial optimization model for truck-and-drone delivery planning. Our problem is at the intersection of the literature on truck-and-drone delivery planning and drone-flight physics, and our solution approach uses machine learning to accelerate transport logistics planning. Section 2.1 summarizes the related literature on truck-and-drone delivery planning, while Section 2.2 reviews the work on drone-flight physics modeling. Section 2.3 reviews the key concepts and advances in machine learning to optimize transport logistics. Due to the large volume of literature in each of these areas, our objective is not to provide a comprehensive review. Instead, we focus on identifying the salient themes and positioning our work in their context.

2.1. Truck-and-Drone Delivery Planning

We can organize the literature on truck-and-drone delivery planning in terms of the various system configurations being considered, the mathematical formulations used, and the solution approaches employed.

System Configurations: Murray and Chu (2015) introduced optimization for collaborative delivery with a single truck and a single drone, a configuration adopted by many researchers (Bouman et al. 2018, Ha et al. 2018, Marinelli et al. 2018, Liu et al. 2019, Poikonen and Golden 2020, de Freitas and Penna 2020, Luo et al. 2022, Jeong and Lee 2023). Other studies have considered different setups, including multiple drones with one truck (Kitjacharoenchai et al. 2019, Murray and Raj 2020, Raj and Murray 2020, Luo et al. 2021, Salama and Srinivas 2022, Jeong and Lee 2023) and multiple drones with multiple trucks (Kitjacharoenchai et al. 2020, Masmoudi et al. 2022, Yu et al. 2024, Gao et al. 2023, Rave et al. 2023, Kloster et al. 2023). Leon-Blanco et al. (2022) allowed drones to visit more than one delivery node per flight.

Despite these differences, the primary goal of most models is to generate routing plans that use truck(s) and drone(s) to visit a specified set of delivery locations to optimize certain objectives. Although most studies use delivery locations directly as nodes in their models, some others also include auxiliary nodes under different names, such as auxiliary or intermediate depot, microdepot, central distribution center or flying warehouse (Jeong et al. 2020, Salama and Srinivas 2022, Jeong and Lee 2023, Rave et al. 2023).

Truck-and-drone models typically approximate travel distances and travel times for both trucks and drones using straight-line Euclidean distances. Some studies estimate travel times that vary depending on the conditions of the road network (Wang et al. 2022), or incorporate traffic congestion and related uncertainty to formulate robust truck-and-drone delivery routes (Yang et al. 2023). Additional practical considerations include the effect of wind on drone flight (Sorbelli et al. 2023) and delivery service times (Das et al. 2020, Yang et al. 2023). Most studies allow drones to take off or land on a truck only at a delivery node or an auxiliary node. To account for recent advances in drone technology, some studies allow drones to take off and land on a moving truck anywhere along the truck path (Li et al. 2022, Thomas et al. 2023). We focus on a setting with one truck and one drone with the drone allowed to visit one delivery node per flight. Like

most previous studies, we model delivery locations directly as model nodes. Additionally, we also account for restricted airspaces and allow the drone to take off and land when the truck is in motion or at rest.

Collaborative truck-and-drone systems have been proposed for a variety of applications, including medical emergencies (Lin et al. 2022), disaster relief (Jeong et al. 2020), entertainment broadcasting (Ayranci 2016), and surveillance (Zeng et al. 2022). However, they are most commonly associated with commercial package delivery, which is the main focus of our work. We refer the reader to the review by Moshref-Javadi and Winkenbach (2021) focusing on logistics applications and those by Chung et al. (2020) and Madani and Ndiaye (2022) for a broader overview of truck-and-drone systems with more general classifications.

Mathematical Formulations: The most common objective functions include the minimization of the total cost or the total duration of the tour. Some studies aim to optimize customer waiting time (Moshref-Javadi et al. 2020, 2021), operational cost (Gao et al. 2023, Rave et al. 2023), total cost to operators and users (Choi and Schonfeld 2021), weighted travel distance by vehicle type (Amorosi et al. 2021), or total travel cost and customer satisfaction (Das et al. 2020). Many existing studies use an arc-based modeling approach, which builds truck-and-drone trajectories by choosing whether or not to include each potential arc to connect a pair of nodes. Several others have adopted the operation-based approach of Agatz et al. (2018). We also use the operation-based modeling approach to minimize the total duration of the tour.

Solution Approaches: Even with simplified drone physics, off-the-shelf solvers are typically unable to handle real-world truck-and-drone delivery planning problems. Therefore, many researchers have developed custom solution methods. These include exact approaches (Amorosi et al. 2021, Roberti and Ruthmair 2021, de Freitas et al. 2023, Yang et al. 2023) and several heuristics such as the genetic algorithm (Remer and Malikopoulos 2019, Das et al. 2020), simulated annealing (Moshref-Javadi et al. 2020, Salama and Srinivas 2022), metaheuristics (Amorosi et al. 2021), neighborhood search (de Freitas et al. 2023, Rave et al. 2023), local search (Wang et al. 2022), column generation-based heuristics (Gao et al. 2023), and multi-agent heuristics (Leon-Blanco et al. 2022). The exact methods do not scale well—for example, the one proposed by Agatz et al. (2018) is tractable for instances with up to 12 nodes, although more than 100 nodes are common in practical package delivery planning problems. To address this challenge, we propose an end-to-end solution approach that scales well with increasing problem size and outperforms all tested benchmarks, consistently and substantially.

2.2. Drone Flight Physics Modeling and Trajectory Planning

Last-mile drone delivery has received considerable attention in recent years. Garg et al. (2023) review these drone applications, while Macrina et al. (2020) provide a broad overview of drone usage in other contexts. Pasha et al. (2022) review different modeling strategies for drone applications. Trajectory planning models vary in terms of the degree to which they account for physics and technical details (Fügenschuh et al. 2021). Some studies accurately model the physical properties of drones (Ładyżyńska-Kozdraś 2012), while

others simplify them to prioritize other optimization objectives and handle larger instances (Abdelhafiz et al. 2010, Pohl and Lamont 2008). Most of the existing work on drone modeling lies somewhere between these two ends (Borrelli et al. 2006, Jun and D’Andrea 2003, Geiger et al. 2006). Schmidt and Fügenschuh (2023) present a mission and flight planning model, with a bilevel time structure to generate a smooth and practical drone trajectory. By linearizing the nonlinear constraints in their mixed-integer nonlinear optimization model, they solve the problem tractably using commercial solvers.

2.3. Machine Learning to Optimize Transport Logistics Planning

For larger and more complex optimization problem instances, solution approaches in the planning of transport and logistics operations must balance tractability with solution quality. Several studies have integrated machine learning (ML) to accelerate optimization (Bengio et al. 2021). ML can be integrated into an optimization algorithm in multiple ways. One approach is to fully replace the optimization problem using ML, where the ML model trained on example problems and solutions directly outputs the final solutions to new instances (Larsen et al. 2018). Another approach is to use ML to augment large-scale optimization to enable more tractable decision-making (Rashedi et al. 2025, Hizir et al. 2025). A third strategy embeds the ML model within the optimization algorithm, repeatedly querying it for local decisions that improve the overall solution process (Khalil et al. 2017). This paper falls into the second category, where we use ML to augment or configure optimization to obtain high-quality solutions quickly.

Bengio et al. (2021) categorize ML-based optimization techniques by their properties. For well-defined large-scale optimization problems that require runtime improvement, methods that mimic or approximate solution patterns are ideal (Gasse et al. 2019, Reiter et al. 2024). In contrast, if the problem is challenging because certain expert knowledge is difficult to formalize or obtain, policy-based approaches that provide deeper insight into optimal solution structures are more suitable (Marcos Alvarez et al. 2014). This paper falls into the first group—we develop neural network predictors to approximate drone travel times and use these estimates to inform optimization via instance-specific inputs.

3. Model

Agatz et al. (2018) defined an “operation” as a combination of a start node, an end node, at most one node served by the drone, and sequence of a non-negative number of nodes visited by either the truck alone or the truck-and-drone jointly (with drone resting on truck). Their model selects the operations that collectively form the final tour. They proposed an exact solution approach that is tractable for instances with up to 12 nodes. Kundu et al. (2022) proposed a polynomial-time splitting algorithm combined with local search that produces high-quality solutions quickly and scales to larger instances of the Agatz et al. (2018) model.

Like many previous studies, Agatz et al. (2018) and Kundu et al. (2022) assume that drone travel times are readily available, although estimating drone travel times is complicated in practice. Moreover, their models

do not provide actual drone trajectories nor guarantee that an operation can be performed within its estimated time. To address these limitations, we introduce a new two-level formulation that improves solution quality and ensures the feasibility of the resulting truck-and-drone operations. Our model also allows the drone to take off or land on the truck anywhere along its path, reinforcing the modeling compatibility with drone technology. This capability further reduces travel time and drone energy consumption. We expand the definition of an operation from Agatz et al. (2018) to allow the drone to take off or land on a moving truck. Our model also prohibits the drone from entering restricted airspaces, according to local regulations.

3.1. Problem Setup and Modeling Assumptions

Our setup considers a system of one truck and one drone to deliver packages to customers while minimizing the duration of the tour. Both vehicles begin at a depot node with the drone resting on the truck and all packages loaded on the truck. Our model makes the following assumptions.

- The drone visits at most one delivery location in each operation. An operation begins when at least one vehicle departs from the operation’s start node and ends when both vehicles reach the operation’s end node. If the drone arrives first, it hovers to wait for the truck. If the truck arrives first, it waits for the drone.
- While resting on the truck, the drone is powered off. The drone battery is sufficient for its assigned tasks due to the sufficient battery capacity, the availability of charging on the truck, or battery swapping.
- To avoid conflict with ground traffic, the drone flies at a fixed altitude consistent with local regulations. It begins flight at the altitude of the truck bed, ascends and cruises at the target altitude, eventually descends to ground level and reaches zero velocity to drop off the package, and similarly returns to the truck.
- The truck driver or drone can easily locate and retrieve packages to serve any delivery node. Each delivery location corresponds to a single package. In case of multiple packages or multiple customers sharing a location, we redefine them as an aggregated single package for each location for modeling convenience.
- The truck travels at known speeds on each segment of the road, but different segments can have different speeds. So, the velocity vector of the truck is known for every segment of the road network.
- During the tour, the truck driver can park the truck at the delivery locations and the drone can fly to serve other delivery locations. Additionally, the drone is allowed to take off and land on the truck at any point during the truck’s journey, including when the truck is in motion.
- The service time spent at each delivery location is negligible and hence omitted from the tour duration.
- In case of multiple solutions minimizing the duration of the operation, the optimal solution with the least drone energy consumption is used. Such ties are common in practice, making this tiebreaker important.
- The service area assigned to a truck-and-drone pair, the topology of the road network, and restricted airspaces are known well before the day of the tour. However, exact delivery locations are available only minutes or hours before the tour. So, ML models can be trained offline days ahead of operations, but route plans must be generated within minutes of obtaining the exact delivery locations for a given day’s tour.

- Before a tour starts, the planner assigns sequences of nodes to the truck and the drone, but the exact trajectory of each flight is adjustable until that operation starts. This places a tighter runtime requirement on overall tour planning, but allows finalizing drone trajectories even after the truck-and-drone tour has started.

3.2. Truck-and-Drone Tour Planning Model (TaDTPM)

The overall truck-and-drone tour planning problem decomposes into two sets of decisions. The upper level assigns delivery nodes to each vehicle and determines the visit sequences. The lower level decides the drone trajectories for all flights. The two levels are interdependent because the drone travel times decided by the lower-level drone trajectory model affect the total tour duration objective function of the upper-level model.

Table 1: Upper-level model notation.

Symbol	Type	Description
\mathcal{U}	Set	Nodes, including the delivery nodes, and the depot where the tour starts and ends
\mathcal{O}	Set	Feasible operations
$\mathcal{O}^-(u) \subseteq \mathcal{O}$	Set	Feasible operations that start at node $u \in \mathcal{U}$
$\mathcal{O}^+(u) \subseteq \mathcal{O}$	Set	Feasible operations that end in node $u \in \mathcal{U}$
$\mathcal{O}(u) \subseteq \mathcal{O}$	Set	Feasible operations that contain node $u \in \mathcal{U}$
$\overline{\mathcal{O}}(\mathcal{S}) \subseteq \mathcal{O}$	Set	Feasible operations that start at a node in $\mathcal{U} \setminus \mathcal{S}$ and end in a node in $\mathcal{S} \subseteq \mathcal{U}$.
u_0	Par.	Depot node.
n	Par.	Number of delivery nodes.
x_o	Var.	Binary. Indicates whether operation $o \in \mathcal{O}$ is performed.
y_u	Var.	Binary. Indicates whether at least one operation starts at node $u \in \mathcal{U}$.
t_o	Var.	Cont. Total duration of operation $o \in \mathcal{O}$.
g_o^T	Var.	Cont. Drone energy consumed in operation $o \in \mathcal{O}$.

Table 1 lists the notation in the upper-level model, Model (1), which is an extension of the model of Agatz et al. (2018). Model (1) is a lexicographic optimization model, which primarily minimizes tour duration, and from all duration-minimizing solutions, it secondarily chooses a solution that minimizes drone energy consumption. Compared to the linear objective in Agatz et al. (2018), our primary objective, Equation (1a), is a product of two variables. Agatz et al. (2018) assume operation times (denoted by t_0) to be constants, which makes the objective linear, while they are decision variables in our Model (1) creating nonlinearity. In addition to this primary objective of total duration (TD) minimization, our model breaks the ties by introducing a secondary objective of minimizing drone energy consumption (DEC), Equation (1b), which is also nonlinear for similar reasons. Section 3.3 describes how the lower-level model computes t_0 and g_o^T .

Our model is based on the idea of an operation, defined as a segment of the overall truck-and-drone tour. The complete tour is a sequence of operations. Each operation starts at a start node with the drone on the truck and ends in an end node, again with the drone on the truck. An operation includes zero or one drone-only delivery node, plus any sequence of a non-negative integer number of truck nodes (visited by the truck alone or by the truck with the drone resting on top of it). Unlike Agatz et al. (2018), our definition of an operation allows the drone to take off and land on the truck, even while it is in motion between nodes.

Constraints (1c)-(1h) are similar to those in Agatz et al. (2018). Constraints (1c) ensure that all nodes are served. Constraints (1d) define y_u so that if at least one operation ends at node u , then at least one operation must start there. Constraints (1e) enforce the flow balance of the operations at each node. Constraints (1f) eliminate sub-tours. Constraints (1g) and (1h), respectively, require that at least one operation ends and starts at the depot node. Finally, the constraints (1i) and (1j) define the domains of the decision variables.

$$\text{Primary:} \quad \text{Minimize} \quad \sum_{o \in \mathcal{O}} t_o \cdot x_o \quad (1a)$$

$$\text{Secondary:} \quad \text{Minimize} \quad \sum_{o \in \mathcal{O}} g_o^T \cdot x_o \quad (1b)$$

$$\sum_{o \in \mathcal{O}^+(u)} x_o \geq 1 \quad \forall u \in \mathcal{U} \quad (1c)$$

$$\sum_{o \in \mathcal{O}^+(u)} x_o \leq n \cdot y_u \quad \forall u \in \mathcal{U} \quad (1d)$$

$$\sum_{o \in \mathcal{O}^+(u)} x_o = \sum_{o \in \mathcal{O}^-(u)} x_o \quad \forall u \in \mathcal{U} \quad (1e)$$

$$\sum_{o \in \overline{\mathcal{O}}(\mathcal{S})} x_o \geq y_u \quad \forall \mathcal{S} \subset \mathcal{U} \setminus \{u_0\}, u \in \mathcal{S} \quad (1f)$$

$$\sum_{o \in \mathcal{O}^+(u_0)} x_o \geq 1 \quad (1g)$$

$$y_{u_0} = 1 \quad (1h)$$

$$x_o \in \{0, 1\}, t_o, g_o^T \in \mathbb{R}_{\geq 0} \quad \forall o \in \mathcal{O} \quad (1i)$$

$$y_u \in \{0, 1\} \quad \forall u \in \mathcal{U} \quad (1j)$$

3.3. Drone Trajectory Model

The lower-level model—an extension of the model of Schmidt and Fügenschuh (2023)—optimizes the trajectory of the drone by coordinating with the location and velocity of the truck at take-off and landing. For each operation, this model takes as input an ordered set of truck delivery nodes (including operation start and end nodes) and a single drone delivery node, and produces the drone's trajectory, travel time, and energy consumption. It synchronizes the drone's trajectory and the truck's path at take-off and landing to allow take-off and landing anywhere along the truck's path. We discretize the planning horizon into time steps called *major time steps*, and each major time step further consists of n_f minor time steps, creating a two-level time discretization. The position, velocity, and acceleration of the drone are modeled in a fine-grained manner at each minor time step to ensure a high degree of modeling accuracy. On the other hand, variables describing the status of the drone (airborne or not) and its relative position with respect to the delivery location are modeled more coarsely using the major time steps to ensure tractability. This two-level discretization is a major contributor to the overall tractability and accuracy of the model. The reader is referred to Schmidt and Fügenschuh (2023) for more details on this trade-off.

Table 2: Lower-level model set notation.

Symbol	Index	Definition
\mathcal{L}	i	Drone altitude bands
\mathcal{V}	j	Drone throttle bands
\mathcal{Q}	q	Restricted airspaces
$\mathcal{T} = \{0, n_f, \dots, n_f \cdot (T - 1)\}$	t	Major time steps
$\mathcal{T}^- = \{0, n_f, \dots, n_f \cdot (T - 2)\}$	t	Major time steps excluding the last one
$\mathcal{T}_f = \{0, 1, \dots, n_f \cdot T - 1\}$	t	Minor time steps
$\mathcal{T}_f^- = \{0, 1, \dots, n_f \cdot T - 2\}$	t	Minor time steps excluding the last one

Table 3: Lower-level model notation for parameters.

Symbol	Description
n_f	Number of minor time steps in a major time step.
T	Number of major time steps in the overall planning horizon.
\tilde{T}	Last minor time step, $\tilde{T} = n_f \cdot T - 1$.
Δ_f	Length of a minor time step.
P_i	Coordinate $i \in \{x, y, z\}$ of the drone delivery location.
λ_2	2D linearization constant = 0.3363788020.
λ_3	3D linearization constant = 0.2980450507.
δ	Maximum distance of drone to delivery node within which the node is considered visited.
\bar{h}	Maximum flight altitude of drone.
\underline{h}	Minimum flight altitude of drone.
h^{min}	Minimum altitude of an airborne drone.
R_i^0	Starting location of the drone along coordinate $i \in \{x, y, z\}$.
$R_i^{\tilde{T}}$	Ending location of the drone along coordinate $i \in \{x, y, z\}$.
Δ	Length of a major time step.
M	A sufficiently large number.
$\bar{v}^{z+}, \bar{v}^{z-}$	Maximum climb and descent rates, respectively, of the drone.
\bar{v}, \bar{a}	Maximum velocity and maximum acceleration, respectively, of the drone.
F	Maximum drone energy level.
m_v	Minimum drone charge level.
ξ	Surplus (relative to horizontal flight) energy consumption rate per unit time per unit climb rate.
η_{ij}	Energy consumption of the drone per unit time in the altitude band $i \in \mathcal{L}$, throttle band $j \in \mathcal{V}$.
θ_j	Discretized drone velocity value in throttle band $j \in \mathcal{V}$.
H_i	Upper limit on the drone altitude in the altitude band $i \in \mathcal{L}$, where the default H_0 is 0.
N_q^Q	Number of halfspaces whose intersection defines the q^{th} RAS for $q \in \mathcal{Q}$.
c_{qni}	Constant multiplier of n^{th} half-space of q^{th} RAS, along i^{th} coordinate, for $q \in \mathcal{Q}, n \in \{1, \dots, N_q^Q\}, i \in \{x, y, z\}$.
c_{qn}^{RHS}	Right hand side constant for n^{th} half-space of q^{th} RAS, for $q \in \mathcal{Q}, n \in \{1, \dots, N_q^Q\}, i \in \{x, y, z\}$.
t_o^{trT}	Truck travel time for operation o .
Z^{TR}	Truck driving altitude.
t_o^*	Optimized total duration of the truck-and-drone operation $o \in \mathcal{O}$.
$\lfloor t \rfloor$	Major time step corresponding to minor time step $t \in \mathcal{T}_f$.
PT_{it}	Coordinate $i \in \{x, y\}$ of truck location at minor time step $t \in \mathcal{T}_f$.
VT_{it}	Truck velocity along coordinate $i \in \{x, y\}$ and minor time steps $t \in \mathcal{T}_f$.

Table 4: Lower-level model notation for decision variables. Note: Drone position vector is relative to delivery location.

Symbol	Description
b_t	Binary. Whether the drone is flying at major time step $t \in \mathcal{T}$.
b_t^+	Binary. Whether drone has started flying at or before the major time step $t \in \mathcal{T}$.

Continuation of Table 4

Symbol	Description
b_t^-	Binary. Whether the drone is available to fly and has not yet finished its flight at major time step $t \in \mathcal{T}$.
w_{it}	Cont. Component $i \in \{x, y, z\}$ of drone's position relative to delivery location at major time step $t \in \mathcal{T}$.
w_{it}^A	Cont. Absolute value of drone position vector's component $i \in \{x, y, z\}$ at major time step $t \in \mathcal{T}$.
w_t^∞	Cont. Maximum absolute value of the drone's 3D position vector components at major time step $t \in \mathcal{T}$.
w_t^{L2}	Cont. Euclidean norm of the 3D position vector of the drone at major time step $t \in \mathcal{T}$.
w_t^M	Cont. Maximum absolute value of horizontal components of drone's 2D position vector at major step $t \in \mathcal{T}$.
w_t^{LA}	Binary. Whether absolute value of the y component of the drone's position vector is larger than or equal to that of the x component at major time step $t \in \mathcal{T}$.
w_t^{LB}	Binary. Whether the absolute value of the z component of the drone's position vector at major time step $t \in \mathcal{T}$ is larger than or equal to those of both the x and y components.
w_{it}^D	Binary. Whether i^{th} component of drone's position vector is negative at major time step $t \in \mathcal{T}$ for $i \in \{x, y, z\}$.
d_t	Binary. Whether the drone visits the delivery location at major time step $t \in \mathcal{T}$.
s_{ijt}	Binary. Whether the drone is in altitude band $i \in \mathcal{L}$ and throttle band $j \in \mathcal{V}$ at major time step $t \in \mathcal{T}$.
f_{qnt}	Binary. Whether the drone is on the safe side of hyperplane $n \in \{1, \dots, N_q^O\}$ of RAS $q \in \mathcal{Q}$ at major time step $t \in \mathcal{T}$. To be outside of the RAS, the drone needs to be on the safe side of at least one hyperplane of that RAS.
$v_t^{\bar{z}+}$	Cont. Climb rate of the drone at minor time step $t \in \mathcal{T}_f$. It is set to zero when the drone is descending.
$v_t^{\bar{z}-}$	Cont. Descent rate of the drone at minor time step $t \in \mathcal{T}_f$. It is set to zero when the drone is climbing.
v_{it}	Cont. Horizontal coordinate $i \in \{x, y\}$ of the drone velocity at minor time step $t \in \mathcal{T}_f$.
v_{it}^A	Cont. Absolute value of component $i \in \{x, y\}$ of drone velocity at minor time step $t \in \mathcal{T}_f$.
v_t^∞	Cont. Maximum absolute value of the horizontal components of drone's velocity at minor time step $t \in \mathcal{T}_f$.
v_t^{L2}	Cont. l_2 norm of the horizontal velocity of the drone at minor time step $t \in \mathcal{T}_f$.
v_t^M	Binary. Whether y component is the largest component of drone's horizontal velocity at minor time step $t \in \mathcal{T}_f$.
v_{it}^D	Binary. Whether the component $i \in \{x, y\}$ of drone velocity is negative at minor time step $t \in \mathcal{T}_f$.
a_{it}	Cont. Horizontal acceleration of the drone at minor time step $t \in \mathcal{T}_f$ along the component $i \in \{x, y\}$.
a_{it}^A	Cont. Absolute value of components $i \in \{x, y\}$ of horizontal acceleration of drone at minor time step $t \in \mathcal{T}_f$.
a_t^∞	Cont. Maximum absolute value of horizontal components of drone's acceleration at minor time step $t \in \mathcal{T}_f$.
a_t^{L2}	Cont. l_2 norm of the horizontal acceleration of the drone at minor time step $t \in \mathcal{T}_f$.
a_t^M	Binary. Whether y component is the largest component of the drone's horizontal acceleration at $t \in \mathcal{T}_f$.
a_{it}^D	Binary. Whether the components $i \in \{x, y\}$ of drone acceleration is negative at minor time step $t \in \mathcal{T}_f$.
r_{it}	Cont. The position of the drone along coordinate $i \in \{x, y, z\}$ at minor time step $t \in \mathcal{T}_f$.
g_t	Cont. The amount of energy consumption of the drone at minor time step $t \in \mathcal{T}_f$.

Tables 2, 3 and 4 define the sets, parameters, and decision variables, respectively, for this lower-level model. We now present the lower-level model for an operation $o \in \mathcal{O}$ in detail. Objective (2a) is to minimize the total duration of the operation, which is defined by constraints (2b)-(2c). Constraints (2b) force t_o to be at least equal to the end of the last major time step during which the drone is in the air, while the constraint (2c) ensures that t_o is at least equal to the duration of the truck for operation. Constraints (3a)-(3c) match the location and horizontal velocity vectors of the truck and drone whenever the drone rests on the truck. Constraints (4a)-(4b) (constraints (4c)-(4d)) ensure that the location (velocity) of the drone is updated depending on whether the drone is resting on the truck or flying. If the drone is airborne during at least one of the major time steps $\llbracket t \rrbracket$ and $\llbracket t + 1 \rrbracket$, then it must follow standard kinematic laws. Constraints (5a) ensure that $b_t = 1$ if and only if both b_t^+ and b_t^- are 1. Constraints (5b) and (5c) allow the drone to have a single transition from non-airborne to airborne status and a single transition from airborne to non-airborne status, respectively.

$$\min t_o \quad (2a)$$

$$(t + n_f) \cdot \Delta_f \cdot b_t \leq t_o \quad \forall t \in \mathcal{T} \quad (2b)$$

$$t_o^{trT} \leq t_o \quad (2c)$$

$$Z^{TR} - M \cdot b_{\lfloor t \rfloor} \leq r_{zt} \leq Z^{TR} + M \cdot b_{\lfloor t \rfloor} \quad \forall t \in \mathcal{T}_f \quad (3a)$$

$$PT_{it} - M \cdot b_{\lfloor t \rfloor} \leq r_{it} \leq PT_{it} + M \cdot b_{\lfloor t \rfloor} \quad \forall i \in \{x, y\}, t \in \mathcal{T}_f \quad (3b)$$

$$VT_{it} - M \cdot b_{\lfloor t \rfloor} \leq v_{it} \leq VT_{it} + M \cdot b_{\lfloor t \rfloor} \quad \forall i \in \{x, y\}, t \in \mathcal{T}_f \quad (3c)$$

$$r_{it} + \Delta_f v_{it} + \frac{\Delta_f^2}{2} a_{it} - M(1 - b_{\lfloor t+1 \rfloor}) \leq r_{i,t+1} \leq r_{it} + \Delta_f v_{it} + \frac{\Delta_f^2}{2} a_{it} + M(1 - b_{\lfloor t+1 \rfloor}) \quad \forall i \in \{x, y\}, t \in \mathcal{T}_f^- \quad (4a)$$

$$r_{it} + \Delta_f v_{it} + \frac{\Delta_f^2}{2} a_{it} - M(1 - b_{\lfloor t \rfloor}) \leq r_{i,t+1} \leq r_{it} + \Delta_f v_{it} + \frac{\Delta_f^2}{2} a_{it} + M(1 - b_{\lfloor t \rfloor}) \quad \forall i \in \{x, y\}, t \in \mathcal{T}_f^- \quad (4b)$$

$$v_{it} + \Delta_f a_{it} - M(1 - b_{\lfloor t+1 \rfloor}) \leq v_{i,t+1} \leq v_{it} + \Delta_f a_{it} + M(1 - b_{\lfloor t+1 \rfloor}) \quad \forall i \in \{x, y\}, t \in \mathcal{T}_f^- \quad (4c)$$

$$v_{it} + \Delta_f a_{it} - M(1 - b_{\lfloor t \rfloor}) \leq v_{i,t+1} \leq v_{it} + \Delta_f a_{it} + M(1 - b_{\lfloor t \rfloor}) \quad \forall i \in \{x, y\}, t \in \mathcal{T}_f^- \quad (4d)$$

$$b_t = b_t^+ + b_t^- - 1 \quad \forall t \in \mathcal{T} \quad (5a)$$

$$b_t^+ \leq b_{t+1}^+ \quad \forall t \in \mathcal{T}^- \quad (5b)$$

$$b_{t+1}^- \leq b_t^- \quad \forall t \in \mathcal{T}^- \quad (5c)$$

Constraints (6a) define the distance vector from the delivery node to the current location of the drone at each major time step. Constraints (6b) require that, when the drone *visits* a delivery node, it is within a predefined distance from the delivery location. Constraint (6c) ensures that the delivery location is visited exactly once during the drone flight. Constraints (7a) establish the upper and lower altitude limits for the drone, while constraints (7b) require that, except when delivering a package or at the start/end of its flight, the drone must remain above the minimum altitude required for airborne operations. Constraints (8a)-(8b) ensure that the operation starts and ends at the correct locations. Constraints (8c)-(8e) set the location and velocity of the drone along the z axis and enforce upper limits on the climb rate and descent rate. Constraints (8f) and (8g) enforce the upper limits of the drone's velocity and acceleration and ensure that the velocity and acceleration are set to zero when the drone is not airborne. Constraints (9a) define the upper and lower limits of drone energy consumption to ensure that the state of charge stays in the allowable range. Constraint (9b) initializes the energy consumption of the drone at 0% of its capacity at the beginning of the operation. Constraints (9c) update the energy consumption of the drone at each minor time step. Constraints (9d) require that the drone is airborne if and only if it belongs to exactly one combination of the altitude band and throttle band at each major time step. Constraints (9e) and (9f), respectively, ensure that the correct throttle band and the correct altitude band are selected at each minor time step. Constraints (10a)-(10b) prevent the drone from entering restricted airspace (RAS). Note that q^{th} RAS is defined by $\{\mathbf{r} \in \mathbb{R}^3 : \forall n \in \{1, \dots, N_q^Q\}, \sum_{i \in \{x, y, z\}} c_{qni} \cdot r_i < c_{qn}^{RHS}\}$.

$$w_{it} = r_{it} - P_i \quad \forall i \in \{x, y, z\}, t \in \mathcal{T} \quad (6a)$$

$$w_t^{L2} \leq \delta + M \cdot (1 - d_t) \quad \forall t \in \mathcal{T} \quad (6b)$$

$$\sum_{t \in \mathcal{T}} d_t = 1 \quad (6c)$$

$$\underline{h} \cdot b_{\llbracket t \rrbracket} \leq r_{zt} \leq \bar{h} \cdot b_{\llbracket t \rrbracket} \quad \forall t \in \mathcal{T}_f \quad (7a)$$

$$r_{zt} \geq h^{\min} \cdot b_{\llbracket t \rrbracket} - M \cdot d_{\llbracket t \rrbracket} \quad \forall t \in \mathcal{T}_f \setminus \{0\} \quad (7b)$$

$$r_{i0} = R_i^0 \quad \forall i \in \{x, y, z\} \quad (8a)$$

$$r_{iT} \geq R_i^T \quad \forall i \in \{x, y, z\} \quad (8b)$$

$$r_{z,t+1} = r_{z,t} + \Delta_f \cdot (v_t^{z+} - v_t^{z-}) \quad \forall t \in \mathcal{T}_f \quad (8c)$$

$$v_t^{z+} \leq \bar{v}^{z+} \quad \forall t \in \mathcal{T}_f \quad (8d)$$

$$v_t^{z-} \leq \bar{v}^{z-} \quad \forall t \in \mathcal{T}_f \quad (8e)$$

$$v_t^{L2} \leq \bar{v} \cdot b_{\llbracket t \rrbracket} \quad \forall t \in \mathcal{T}_f \quad (8f)$$

$$a_t^{L2} \leq \bar{a} \cdot b_{\llbracket t \rrbracket} \quad \forall t \in \mathcal{T}_f \quad (8g)$$

$$0 \leq g_t \leq F - m_v \quad \forall t \in \mathcal{T}_f \quad (9a)$$

$$g_0 = 0 \quad (9b)$$

$$g_{t+1} = g_t + \Delta_f (\xi * v_t^{z+} + \sum_{i \in \mathcal{L}, j \in \mathcal{V}} \eta_{ij} s_{ij\llbracket t \rrbracket}) \quad \forall t \in \mathcal{T}_f^- \quad (9c)$$

$$\sum_{i \in \mathcal{L}, j \in \mathcal{V}} s_{ijt} = b_t \quad \forall t \in \mathcal{T} \quad (9d)$$

$$v_t^{L2} - M \cdot (1 - b_{\llbracket t \rrbracket}) \leq \sum_{i \in \mathcal{L}, j \in \mathcal{V}} \theta_j s_{ij\llbracket t \rrbracket} \leq v_t^{L2} + M \cdot (1 - b_{\llbracket t \rrbracket}) \quad \forall t \in \mathcal{T}_f \quad (9e)$$

$$\sum_{i \in \mathcal{L}} H_{i-1} \sum_{j \in \mathcal{V}} s_{ij\llbracket t \rrbracket} - M \cdot (1 - b_{\llbracket t \rrbracket}) \leq r_{zt} \leq \sum_{i \in \mathcal{L}} H_i \sum_{j \in \mathcal{V}} s_{ij\llbracket t \rrbracket} + M \cdot (1 - b_{\llbracket t \rrbracket}) \quad \forall t \in \mathcal{T}_f \quad (9f)$$

$$\sum_{i \in \{x, y, z\}} c_{qni} \cdot r_{it} \geq c_{qn}^{RHS} - M(1 - f_{qn\llbracket t \rrbracket}) \quad \forall q \in \mathcal{Q}, n \in \{1, \dots, N_q^0\}, t \in \mathcal{T}_f \quad (10a)$$

$$\sum_{n=1}^{N_q^0} f_{qnt} \geq 1 \quad \forall q \in \mathcal{Q}, t \in \mathcal{T} \quad (10b)$$

Linearization of the Euclidean Norms: Following Schmidt and Fügenschuh (2023), we approximate Euclidean (l_2) norm by a convex combination of the l_1 and l_∞ norms (Chaudhuri et al. 1992) as $\|x\|_2 = \lambda_2 \|x\|_1 + (1 - \lambda_2) \|x\|_\infty$ in two dimensions and as $\|x\|_2 = \lambda_3 \|x\|_1 + (1 - \lambda_3) \|x\|_\infty$ in three dimensions, where $\|x\|_1$, $\|x\|_2$ and $\|x\|_\infty$ represent the l_1 , l_2 , and l_∞ norms, respectively, of a vector x . Rhodes (1995) estimated the values as $\lambda_2 \approx 0.3363788020$ and $\lambda_3 \approx 0.2980450507$. The l_1 and l_∞ norms themselves are nonlinear, but they can be linearized with further reformulation by defining and using new binary variables. If $v_{it} \forall i \in \{x, y\}$ are the horizontal components of drone velocity at time t , the l_2 norm of the horizontal velocity vector is approximated by $\sqrt{v_{xt}^2 + v_{yt}^2} \approx \lambda_2 \cdot (|v_{xt}| + |v_{yt}|) + (1 - \lambda_2) \cdot \max\{|v_{xt}|, |v_{yt}|\}$. We introduce the absolute value variables $v_{it}^A = |v_{it}|$, $\forall i \in \{x, y\}$, and denote the l_2 and l_∞ norms as $v_t^{L2} = \sqrt{v_{xt}^2 + v_{yt}^2}$, and $v_t^\infty = \max\{|v_{xt}|, |v_{yt}|\}$.

Binary variable $v_t^M = 1$ if $v_t^\infty = v_{yt}^A$, and $v_t^M = 0$ otherwise. Similarly, $v_{it}^D = 0$ if $v_{it}^A = v_{it}$, and $v_{it}^D = 1$ otherwise, $\forall i \in \{x, y\}$. Constraints (11a) approximate the l_2 norm as a linear combination of the l_1 and the l_∞ norms, (11b)-(11d) set $v_t^\infty = \max\{v_{xt}^A, v_{yt}^A\}$, and (11e)-(11h) set $v_{it}^A = |v_{it}|, \forall i \in \{x, y\}$.

$$v_t^{L2} = \lambda_2 \cdot (v_{xt}^A + v_{yt}^A) + (1 - \lambda_2) \cdot v_t^\infty \quad \forall t \in \mathcal{T}_f \quad (11a)$$

$$v_{it}^A \leq v_t^\infty \quad \forall i \in \{x, y\}, t \in \mathcal{T}_f \quad (11b)$$

$$v_t^\infty - M \cdot v_t^M \leq v_{xt}^A \leq v_t^\infty + M \cdot v_t^M \quad \forall t \in \mathcal{T}_f \quad (11c)$$

$$v_t^\infty - M \cdot (1 - v_t^M) \leq v_{yt}^A \leq v_t^\infty + M \cdot (1 - v_t^M) \quad \forall t \in \mathcal{T}_f \quad (11d)$$

$$v_{it} \leq v_{it}^A \quad \forall i \in \{x, y\}, t \in \mathcal{T}_f \quad (11e)$$

$$-v_{it} \leq v_{it}^A \quad \forall i \in \{x, y\}, t \in \mathcal{T}_f \quad (11f)$$

$$v_{it} - M \cdot v_{it}^D \leq v_{it}^A \leq v_{it} + M \cdot v_{it}^D \quad \forall i \in \{x, y\}, t \in \mathcal{T}_f \quad (11g)$$

$$-v_{it} - M \cdot (1 - v_{it}^D) \leq v_{it}^A \leq -v_{it} + M \cdot (1 - v_{it}^D) \quad \forall i \in \{x, y\}, t \in \mathcal{T}_f \quad (11h)$$

If $a_{it} \forall i \in \{x, y\}$ are the horizontal components of drone acceleration at time t , the l_2 norm of the horizontal acceleration vector is approximated by $\sqrt{a_{xt}^2 + a_{yt}^2} \approx \lambda_2 \cdot (|a_{xt}| + |a_{yt}|) + (1 - \lambda_2) \cdot \max\{|a_{xt}|, |a_{yt}|\}$. We define continuous variables $a_{xt}^A, a_{yt}^A, a_t^{L2}, a_t^\infty$, and binary variables $a_t^M, a_{xt}^D, a_{yt}^D$ analogously to the corresponding variables for velocity. Constraints (12a)-(12h) linearize these acceleration relationships.

$$a_t^{L2} = \lambda_2 \cdot (a_{xt}^A + a_{yt}^A) + (1 - \lambda_2) \cdot a_t^\infty \quad \forall t \in \mathcal{T}_f \quad (12a)$$

$$a_{it}^A \leq a_t^\infty \quad \forall i \in \{x, y\}, t \in \mathcal{T}_f \quad (12b)$$

$$a_t^\infty - M \cdot a_t^M \leq a_{xt}^A \leq a_t^\infty + M \cdot a_t^M \quad \forall t \in \mathcal{T}_f \quad (12c)$$

$$a_t^\infty - M \cdot (1 - a_t^M) \leq a_{yt}^A \leq a_t^\infty + M \cdot (1 - a_t^M) \quad \forall t \in \mathcal{T}_f \quad (12d)$$

$$a_{it} \leq a_{it}^A \quad \forall i \in \{x, y\}, t \in \mathcal{T}_f \quad (12e)$$

$$-a_{it} \leq a_{it}^A \quad \forall i \in \{x, y\}, t \in \mathcal{T}_f \quad (12f)$$

$$a_{it} - M \cdot a_{it}^D \leq a_{it}^A \leq a_{it} + M \cdot a_{it}^D \quad \forall i \in \{x, y\}, t \in \mathcal{T}_f \quad (12g)$$

$$-a_{it} - M \cdot (1 - a_{it}^D) \leq a_{it}^A \leq -a_{it} + M \cdot (1 - a_{it}^D) \quad \forall i \in \{x, y\}, t \in \mathcal{T}_f \quad (12h)$$

Finally, the l_2 norm of the drone's position vector at each major time step is approximated by constraints (13a)-(13l) using a strategy similar to that used for velocity and acceleration, except that the position vector is modeled in three dimensions as against the two-dimensional velocity and acceleration vectors modeled above. Another difference is that, as explained earlier, velocity and acceleration are modeled at each minor time step while the drone position relative to the delivery location is modeled at each major time step.

$$w_t^{L2} = \lambda_3 \cdot (w_{xt}^A + w_{yt}^A + w_{zt}^A) + (1 - \lambda_3) \cdot w_t^\infty \quad \forall t \in \mathcal{T} \quad (13a)$$

$$w_t^M \leq w_t^\infty \quad \forall t \in \mathcal{T} \quad (13b)$$

$$w_{zt}^A \leq w_t^\infty \quad \forall t \in \mathcal{T} \quad (13c)$$

$$w_t^\infty - M \cdot w_t^{LB} \leq w_t^M \leq w_t^\infty + M \cdot w_t^{LB} \quad \forall t \in \mathcal{T} \quad (13d)$$

$$w_t^\infty - M \cdot (1 - w_t^{LB}) \leq w_{zt}^A \leq w_t^\infty + M \cdot (1 - w_t^{LB}) \quad \forall t \in \mathcal{T} \quad (13e)$$

$$w_{it}^A \leq w_t^M \quad \forall i \in \{x, y\}, t \in \mathcal{T} \quad (13f)$$

$$w_t^M - M \cdot w_t^{LA} \leq w_{xt}^A \leq w_t^M + M \cdot w_t^{LA} \quad \forall t \in \mathcal{T} \quad (13g)$$

$$w_t^M - M \cdot (1 - w_t^{LA}) \leq w_{yt}^A \leq w_t^M + M \cdot (1 - w_t^{LA}) \quad \forall t \in \mathcal{T} \quad (13h)$$

$$w_{it} \leq w_{it}^A \quad \forall i \in \{x, y, z\}, t \in \mathcal{T} \quad (13i)$$

$$-w_{it} \leq w_{it}^A \quad \forall i \in \{x, y, z\}, t \in \mathcal{T} \quad (13j)$$

$$w_{it} - M \cdot w_{it}^D \leq w_{it}^A \leq w_{it} + M \cdot w_{it}^D \quad \forall i \in \{x, y, z\}, t \in \mathcal{T} \quad (13k)$$

$$-w_{it} - M \cdot (1 - w_{it}^D) \leq w_{it}^A \leq -w_{it} + M \cdot (1 - w_{it}^D) \quad \forall i \in \{x, y, z\}, t \in \mathcal{T} \quad (13l)$$

Finally, the constraints (14a)-(14m) define the domains of the decision variables.

$$v_t^{z+}, v_t^{z-}, v_t^\infty, v_t^{L2}, a_t^\infty, a_t^{L2}, g_t \geq 0 \quad \forall t \in \mathcal{T}_f \quad (14a)$$

$$w_t^\infty, w_t^{L2}, w_t^M \geq 0 \quad \forall t \in \mathcal{T} \quad (14b)$$

$$v_{it}, a_{it} \in \mathbb{R} \quad \forall i \in \{x, y\}, t \in \mathcal{T}_f \quad (14c)$$

$$v_{it}^A, a_{it}^A \geq 0 \quad \forall i \in \{x, y\}, t \in \mathcal{T}_f \quad (14d)$$

$$w_{it} \in \mathbb{R} \quad \forall i \in \{x, y, z\}, t \in \mathcal{T} \quad (14e)$$

$$w_{it}^A \geq 0 \quad \forall i \in \{x, y, z\}, t \in \mathcal{T} \quad (14f)$$

$$r_{it} \in \mathbb{R} \quad \forall i \in \{x, y, z\}, t \in \mathcal{T}_f \quad (14g)$$

$$v_t^M, a_t^M \in \{0, 1\} \quad \forall t \in \mathcal{T}_f \quad (14h)$$

$$b_t, b_t^+, b_t^-, w_t^{LA}, w_t^{LB}, d_t \in \{0, 1\} \quad \forall t \in \mathcal{T} \quad (14i)$$

$$v_{it}^D, a_{it}^D \in \{0, 1\} \quad \forall i \in \{x, y\}, t \in \mathcal{T}_f \quad (14j)$$

$$w_{it}^D \in \{0, 1\} \quad \forall i \in \{x, y, z\}, t \in \mathcal{T} \quad (14k)$$

$$s_{ijt} \in \{0, 1\} \quad \forall i \in \mathcal{L}, j \in \mathcal{V}, t \in \mathcal{T} \quad (14l)$$

$$f_{qu} \in \{0, 1\} \quad \forall q \in \mathcal{Q}, n \in \{1, \dots, N_q^Q\}, t \in \mathcal{T} \quad (14m)$$

In addition to the primary objective function of minimizing duration, we break ties by minimizing drone energy consumption (DEC) as a secondary objective function, modeled by (15a), and defined in constraint (15c). Constraints (15b) ensure that while minimizing DEC, the drone still respects the least duration established by the time-minimizing truck-and-drone model (Equations (2)-(14)). Recall that t_o^* is the optimized total duration of the operation obtained by solving the duration-minimizing truck-and-drone model. Overall, we first set t_o^* at the lowest possible value of t_o given by solving the model (2)-(14). Subsequently, we solve the tie-breaker model, which has the objective function given by the equation (2) and the constraints given by equations (3)-(14), (15b), and (15c).

$$\min g_o^T \quad (15a)$$

$$(t + n_f) \cdot \Delta_f \cdot b_t \leq t_o^* \quad \forall t \in \mathcal{T} \quad (15b)$$

$$g_o^T = g_{\bar{t}} \quad (15c)$$

The total energy consumption of the drone for the entire truck-and-drone tour is the sum of the DEC's of all selected operations. Formally, if g_o^T is the optimal energy consumption of the drone for operation $o \in \mathcal{O}$, then the total drone energy consumption for the entire tour is given by $\sum_{o \in \mathcal{O}} g_o^T \cdot x_o$.

4. Solution Approach

Our two-level decomposition achieves two goals. First, for a given set of lower-level objective function coefficients (namely t_o and $g_o^T, \forall o \in \mathcal{O}$), it ensures that the upper level is a biobjective mixed-integer linear optimization problem. Second, although the lower level is a biobjective mixed-integer nonconvex optimization problem, the decomposition substantially reduces its size: Without the decomposition, the overall optimization problem needs to be solved to jointly obtain the optimal trajectories for *each* candidate operation, whereas the decomposition breaks it down into individual optimization problems, one for each candidate operation. For fixed values of t_o and $g_o^T, \forall o \in \mathcal{O}$, the upper level is a biobjective extension of the mixed-integer linear optimization model of the TSP-D (Agatz et al. 2018). Kundu et al. (2022) proposed a polynomial time splitting algorithm combined with local search for the single-objective TSP-D and produced high-quality solutions to realistic problem sizes. If the objective function coefficients are known beforehand, the TSP-D model can be solved by extending this approach. However, accurate estimation of drone travel times requires solving the lower-level model for all candidate operations, and the number of such operations grows exponentially with the number of delivery locations, making a full enumeration unrealistic.

Instead, we propose a new neural network-based approach to generate accurate estimates of drone travel time for each operation. Kundu et al. (2022) use Euclidean travel distances, which we propose to replace with a neural network (NN). Our NN model is trained on offline data and outputs a drone travel time estimate given the coordinates of three locations: operation start, drone delivery, and operation end. Next, we combine these NN-based estimates with an augmented version of the heuristic by Kundu et al. (2022)

to generate the optimal set of operations. Finally, the detailed lower-level model can be used to provide a feasible 4D (x , y , z , and t) trajectory plan, duration, and DEC for each selected operation. We present our overall solution approach in Section 4.1. Section 4.2 describes the NN design and training process. Section 4.3 presents the drone-only trajectory model used to generate the NN training data. Finally, Section 4.4 provides three methods for calculating drone flight times with varying degrees of simplicity.

4.1. Overall Solution Approach

The algorithm of Agatz et al. (2018) was improved by Kundu et al. (2022) (see Kundu (2022) for implementation details). The general concept behind these solution approaches has been summarized as “order-first split-second” or “route and reassign”. Additionally, since the solution can be improved using an improvement heuristic as a third step, these approaches can be considered “order-first, split-second, improve-third” methods. We also use a “order-first, split-second, improve-third” approach, with the following three steps.

Ordering: In the first step, these approaches assume that the drone does not leave the truck throughout the tour, and instead the truck covers all delivery nodes as parts of a single giant tour. Because this is a TSP, known to be NP-hard, and because the node ordering in this step only indirectly determines the quality of the final truck-and-drone solution, heuristics are typically used to obtain a fast initial TSP solution. Agatz et al. (2018) used the Concorde TSP solver (Applegate 2006), and Kundu (2022) used the Lin-Kernighan-Helsgaun (LKH) algorithm (Helsgaun 2000). We chose to use the two-opt local search heuristic (Croes 1958) for its shorter runtime. We also experimented with other TSP heuristics, but they neither improved the quality of the final truck-and-drone solution nor affected the main conclusions and takeaways.

Splitting: The splitting step evaluates—on the basis of their durations, obtained by the estimation methods in Section 4.4—all possible operations in which the nodes visited by the truck within that operation are in the same order as that induced by the truck-only tour. For this splitting step, Agatz et al. (2018) used an exact dynamic programming-based partitioning method, while Kundu et al. (2022) used a shortest path procedure on a directed acyclic graph to reduce computational overhead without sacrificing optimality. Due to its computational efficiency, we chose the splitting method in Kundu et al. (2022), whose key idea is to keep track of the minimum travel time to reach each node from the start node and update this minimum travel time during the evaluation process whenever new operations with a shorter travel time are encountered. This step provably produces the shortest possible truck-and-drone tour among all tours where the truck visits nodes in the same order as that induced by the truck-only tour from the first step.

Since there are $O(n^3)$ possible operations with the same induced ordering as a given n -node truck-only tour, the evaluation process requires at least $O(n^3)$ runtime. Depending on the method used to calculate the duration of each operation, the overall runtime can be $O(n^4)$ as in the exact partitioning method in Agatz et al. (2018) or $O(n^3)$ as in the speed-up version of the method in Agatz et al. (2018), as well as in the method proposed in Kundu et al. (2022) and Kundu (2022). We use the splitting step as implemented in

Kundu (2022) where the operation time calculation takes $O(1)$ runtime, and thus the splitting step has $O(n^3)$ time complexity. We use this method because it gives higher quality solutions with runtimes of more than 95% lower than the methods in Agatz et al. (2018) for large problem instances (Kundu et al. 2022).

Improvement: Because the truck-and-drone tour obtained by the splitting step depends on the initial truck-only tour, it can be improved by considering alternative truck-only tours to initiate the splitting step. To find “neighbors” of the initial truck-only tour, both Agatz et al. (2018) and Kundu et al. (2022) consider an iterative improvement procedure involving three different methods: one-point move (relocate one node), two-point move (swap two nodes), and two-opt (replace two edges). We run the splitting step on all neighbors of the initial truck-only TSP tour to find their corresponding shortest truck-and-drone tours and pick the best one, which improves the truck-and-drone solution compared to the original single run of the splitting method. See Section 6.3 in Agatz et al. (2018) for more details on this improvement step.

Importantly, unlike Agatz et al. (2018) and Kundu (2022), we do not estimate drone travel times as Euclidean distances divided by a constant speed. Sections 4.2-4.4 detail our estimation method.

4.2. Neural Network Model Predictor for Drone-Only Time Estimation

Computing a specific drone trajectory and travel time requires solving the lower-level model (2)-(14), a calculation repeated several times when solving large-scale problems, which is computationally demanding. We use a NN model to accelerate the runtimes. The input layer of the NN encodes the fundamental descriptors of a drone operation: the x and y coordinates of the drone’s start, delivery, and end locations within an operation, comprising six features. The NN produces one output: drone travel time. To train the NN, we generate instances of operations assuming uniformly distributed locations of all three nodes, and run the drone-only model described in Section 4.3 to obtain the “true” drone travel time labels for each instance. We then pair these labels with the instance’s six-feature vector to build a training dataset for the NN.

We prefer a simple NN structure, with a single hidden layer to reduce the complexity and runtime of the training and tuning processes. A single hidden layer with a sufficient number of neurons can approximate any continuous function, and structures with a single hidden layer are common in regression (Hornik et al. 1989). Moreover, function approximation tasks with high-dimensional data and a large number of neurons generalize well (Zhang et al. 2017). Therefore, we choose to use a neural network with a large single hidden layer. We tune the number of neurons in this hidden layer and other hyperparameters via a standard grid search. For each hyperparameter considered in the grid search, we first refer to the default values from the scikit-learn package called Multilayer Perceptron Regressor, or MLPRegressor, and fine-tune the hyperparameters around these default values. As too few neurons lead to underfitting, while too many can cause overfitting and unnecessary computational cost (Goodfellow et al. 2016), we consider a range of choices (1000, 2500 or 4000 hidden neurons) to balance expressiveness and overfitting risks.

For the activation function, we provide options that are suitable for both near-linear cases (Identity) and nonlinear cases (ReLU) (Glorot et al. 2011) to offer flexibility. The alpha value controls the strength of L2

regularization, with smaller values implying weak regularization which allows the model to fit the training data more closely and risks overfitting, and larger values implying strong regularization which forces the model coefficients to shrink towards zero and reduces model complexity and overfitting. Intermediate values provide a spectrum of regularization strengths to balance between underfitting and overfitting. To find the right balance, we provide options with a range of magnitudes (0.0001, 0.05, 0.5, and 0.8). The choice of learning rate schedule affects the convergence behavior (LeCun et al. 2002, Bengio 2012, Bottou et al. 2018): constant learning schedule maintains a fixed step size for stable but potentially slow convergence; inverse scaling gradually reduces the step size to balance exploration and fine-tuning; and the adaptive learning schedule adjusts dynamically based on gradient changes to improve convergence efficiency. We use these three options in the set of hyperparameters. Table 5 lists the hyperparameter values considered and those selected. We use the ‘‘Adam’’ solver for model training, which is suitable for relatively large datasets like ours (Kingma and Ba 2014). We use mean squared error as the scoring metric, which has smooth differentiability, making it well suited for such gradient-based optimization.

Table 5: Candidate hyperparameter values for NN grid search.

Grid Search Hyperparameter	Candidate Values	Selected Value (no RAS)	Selected Value (with RAS)
Hidden layer size	1000, 2500, 4000	4000	4000
Activation function	Identity, ReLU	ReLU	ReLU
Regularization parameter	0.0001, 0.05, 0.5, 0.8	0.05	0.0001
Learning rate	Constant, Inverse Scaling, Adaptive	Constant	Constant

4.3. Drone-Only Trajectory Model

In order to generate the training data for the NN predictor, we modify the lower-level model as follows.

We remove the constraint (2c) in order to use the total drone travel time as the objective function. In addition, we remove the truck-and-drone coordination constraints (3a)-(3c). Finally, constraints (4a)-(4b) are replaced by constraint (16a), and constraint (4c)-(4d) are replaced by constraint (16b).

$$r_{i,t+1} = r_{it} + \Delta_f \cdot v_{it} + \frac{\Delta^2}{2} \cdot a_{it} \quad \forall i \in \{x, y\}, t \in \mathcal{T}_f^- \quad (16a)$$

$$v_{i,t+1} = v_{it} + \Delta_f \cdot a_{it} \quad \forall i \in \{x, y\}, t \in \mathcal{T}_f^- \quad (16b)$$

4.4. Three Solution Approaches to Estimate Drone Operation Time

We present three methods to calculate the drone travel time with varying degrees of simplicity.

1. Euclidean Distance-Based Method (K method): This method represents the state-of-the-art in drone travel time estimation for truck-and-drone planning. It computes the straight-line distances from the operation start node to the delivery node and the delivery node to the operation end node, and divides the sum of these two distances by an estimated drone speed (70 km/h) to estimate drone travel time.

2. Calibrated Euclidean Distance-Based Method (MK method): This method is an improved version of the state-of-the-art in drone time estimation for truck-and-drone planning. This method generates an offline

training dataset using the process described in Section 4.2, listing the coordinates of the start, delivery, and end nodes, for a training set of operations. We then run the drone-only model (from Section 4.3) on each operation to obtain the drone travel times. Next, we divide this travel time by the Euclidean distance-based drone travel time calculated by the K method to produce an operation-specific correction factor. We calculate the average value of this correction factor over all operations in the training set. For any new operation presented in the online phase, we calculate the drone travel time of the K method, and multiply it by this average correction factor from the training phase to get the final drone travel time estimate.

3. **Neural Network Based Method (P method):** This method trains an NN on the offline training set, and uses the trained NN to estimate drone travel time for any new operation presented in the online phase.

5. Computational Results

We conducted computational experiments for two different scenarios. Scenario I approximates a truck-and-drone service area without tall buildings or mountains, that is, without restricted airspaces (RAS), and with uniformly distributed delivery nodes. Scenario II represents real-world settings with large regions where the truck and drone are not allowed (modeled as RAS), due to tall buildings or mountains, and with uniformly distributed delivery needs in the rest of the service area. The truck is assumed to travel along the shortest path between consecutive nodes avoiding the RAS, if any. In each scenario, we compare the duration and drone energy consumption of the entire truck-and-drone tour for the three solution approaches (K, MK, and P). We vary the number of delivery nodes (across 10, 20, 50, 75, 100, 175, 250) and the average speed of the truck (across 20, 30, 40, 50, 60, 70, 80 km/h). For each combination of scenario, number of nodes, and truck speed, we generate 100 instances with different sets of delivery locations and report average results. Each truck-and-drone tour plan in this section was computed in at most 189 seconds of runtime.

5.1. Scenario I: No Restricted Airspaces

We first quantify the benefits of drone use. Then we evaluate the benefits of our P method compared to benchmark approaches in terms of reduction in tour duration and, finally, in terms of the drone energy saved.

5.1.1. Benefits of Using a Drone: In the conventional delivery logistics, all packages are delivered by the truck on a TSP tour that visits all nodes. To evaluate the extent to which drone usage can reduce tour duration, we compare the durations of truck-only and truck-and-drone tours. We solve the problem of minimizing the truck-only tour duration using the TSP heuristics used in the first step of our overall solution approach, while we minimize the truck-and-drone tour duration using the aforementioned P method. For a given number of nodes and truck speed, let the total durations of the truck-and-drone and truck-only tours for the i^{th} instance (of the 100 instances) be τ_i^P and τ_i^T , respectively. We calculate how frequently the truck-and-drone solution outperforms the truck-only solution as $\sum_{i \in \{1, \dots, 100\}} I(\tau_i^T > \tau_i^P)$ and report it in columns 2-8 in Table 6 and the left sub-figure of Figure 6 in Appendix A. We also calculate the average reduction in

Table 6: Comparing the P method with the Truck-only TSP for Scenario I (without RAS). Columns 2-8 list the number of instances (out of 100) where the P method strictly outperforms the Truck-only TSP in terms of the tour duration. Columns 9-15 list the average percentage reduction in duration by the P method compared to Truck-only TSP.

Metrics		Instances Where P Outperforms Truck-only TSP							Avg. % Reduction in Duration by P method							
Nodes	Speed (km/h)	20	30	40	50	60	70	80	20	30	40	50	60	70	80	
	10		100	99	100	100	99	99	99	25.28	23.49	21.22	17.67	14.00	12.41	11.74
20		100	100	100	100	100	100	99	25.88	24.59	22.15	18.79	15.92	13.90	12.08	
50		100	100	100	100	100	98	100	24.28	22.48	19.23	16.18	13.73	11.88	10.67	
75		100	100	100	100	100	100	100	23.97	21.49	18.13	15.53	13.11	11.23	10.18	
100		100	100	100	100	100	100	100	24.12	21.02	17.90	15.13	12.86	10.90	9.75	
175		100	100	100	100	100	100	100	22.65	19.46	16.18	13.86	11.83	9.86	8.83	
250		100	100	100	100	100	100	100	21.98	18.48	15.29	13.02	11.09	9.04	8.35	

Table 7: Comparing the P method with the K and MK methods on total duration for Scenario I (without RAS). Columns 2-8 (respectively, columns 9-15) list the average percentage reduction by the P method compared to the K (respectively, MK) method. Each row shows a different number of nodes and each column a different truck speed.

Metrics		Avg. % Reduction in Duration by P vs. K							Avg. % Reduction in Duration by P vs. MK							
Nodes	Speed (km/h)	20	30	40	50	60	70	80	20	30	40	50	60	70	80	
	10		0.15	0.73	2.30	4.32	6.78	5.66	3.97	0.02	0.26	0.21	0.95	0.38	0.41	0.69
20		0.25	1.60	4.22	10.56	11.16	8.89	7.09	0.08	0.50	1.37	2.05	1.28	0.97	1.21	
50		0.52	3.84	11.19	18.56	19.78	16.06	13.67	0.30	2.25	6.72	7.21	3.12	3.19	2.70	
75		0.83	5.54	14.67	22.89	24.00	19.70	16.07	0.47	4.23	10.34	10.36	5.61	5.93	4.23	
100		1.41	7.51	18.51	26.06	27.43	21.86	18.57	1.13	5.97	13.24	14.04	7.21	7.05	6.46	
175		3.73	13.96	26.23	33.75	34.08	27.47	23.80	3.33	12.23	21.04	20.65	12.40	11.69	10.55	
250		6.82	20.64	33.23	39.80	38.77	31.21	28.20	6.47	18.74	28.19	26.01	16.17	15.42	14.45	

Table 8: Comparing the P method with the K and MK methods on DEC for Scenario I (without RAS). Columns 2-8 (respectively, columns 9-15) list the average percentage reduction by the P method compared to the K (respectively, MK) method. Each row shows a different number of nodes and each column a different truck speed.

Metrics		Avg. Reduction (%) in DEC by P vs. K							Avg. Reduction (%) in DEC by P vs. MK							
Nodes	Speed (km/h)	20	30	40	50	60	70	80	20	30	40	50	60	70	80	
	10		1.82	3.82	9.38	13.98	22.30	22.65	13.26	-0.80	-1.52	3.25	-1.70	-14.66	-4.24	-6.43
20		2.91	8.17	17.49	25.24	24.60	21.00	17.91	2.16	5.80	12.96	10.34	-1.00	-3.55	-3.92	
50		8.20	21.16	32.36	36.78	35.74	31.13	25.05	7.71	19.70	27.73	24.62	12.26	8.98	6.84	
75		12.99	27.88	37.68	42.86	40.92	33.90	30.31	12.47	26.63	33.43	31.05	19.11	14.34	14.16	
100		18.01	33.20	42.01	46.23	44.17	37.24	33.36	17.79	31.87	37.78	35.58	22.34	18.10	17.53	
175		27.87	43.51	51.48	54.58	52.33	44.53	41.42	27.50	42.21	47.64	43.91	32.86	28.33	26.93	
250		36.13	50.86	57.81	60.40	57.78	49.60	45.03	35.80	49.54	54.14	49.82	38.84	34.31	31.76	

total duration achieved by the truck-and-drone tour compared to the truck-only tour as $\frac{1}{100} \sum_{i \in \{1, \dots, 100\}} \frac{\tau_i^T - \tau_i^P}{\tau_i^T}$ and report it in columns 9-15 in Table 6 and the right sub-figure of Figure 6 in Appendix A.

From these results, we observe that in 43 of the 49 combinations of the number of nodes and truck speed, the truck-and-drone solution has strictly less duration than the truck-only solution for *all* 100 instances.

Across all 4,900 instances, the truck-and-drone solution has strictly less duration than the truck-only solution in 4,893 (that is, 99.86%) instances. The truck-only solution performs as well as the truck-and-drone P method only in a handful of instances with a small number of nodes (50 or less), especially at high truck speeds (70 km/h or higher). High truck speeds dilute the speed advantage of the drone, making the drone less useful. Columns 9-15 in Table 6 show that the drone reduces the tour duration, on average, by 16.38%.

Columns 2-8 in Table 6 show that the duration reduction occurs more frequently at lower truck speeds (which amplify the drone’s speed advantage) and more nodes. On the other hand, columns 9-15 in Table 6 show that the greatest average improvement also occurs at lower truck speeds (as expected), but at *fewer* nodes. At first glance, this observation is somewhat surprising but can be explained as follows. As the number of nodes increases, there are more opportunities for the drone to improve the truck-only TSP solution because there are more candidate drone nodes, and hence many more truck-and-drone operations to explore. So, there is a higher likelihood of finding at least some node that, when assigned to a drone, can reduce the overall travel time. Thus, there is a greater chance to improve the tour using a drone. Therefore, more nodes leads to more frequent duration reduction. But with fewer nodes, the denominator in the calculation of percentage reduction (i.e., the truck-only tour duration) decreases, making any improvement appear larger as a percentage. So, in case of fewer nodes, the delegation of a subset of delivery nodes to the drone yields a higher percentage reduction in tour duration, although the improvement frequency itself is lower.

Overall, the truck-and-drone tour optimized with our P method consistently and substantially outperforms the truck-only tour, especially at low to medium truck speeds, which are common in large congested cities.

5.1.2. Benefits of Our Solution Approach: Table 7 and Figure 7 (in Appendix A) show the average reduction in truck-and-drone tour duration achieved by the P method compared to the K and MK methods. As before, we solve 100 instances for each combination of the number of nodes and truck speed. For the i^{th} instance, let τ_i^P , τ_i^K and τ_i^{MK} be the truck-and-drone tour durations obtained by the P, K and MK method, respectively. Then the average reduction in truck-and-drone tour duration achieved by the P method compared to the K and MK methods is calculated as $\frac{1}{100} \sum_{i \in \{1, \dots, 100\}} \frac{\tau_i^K - \tau_i^P}{\tau_i^K}$ and $\frac{1}{100} \sum_{i \in \{1, \dots, 100\}} \frac{\tau_i^{MK} - \tau_i^P}{\tau_i^{MK}}$.

We observe that in each of the 49 combinations, the P method outperforms both the K and MK methods in terms of tour duration, on average by 15.06% and 7.13%, respectively. The duration reduction increases monotonically as the number of nodes increases. This higher percentage of duration reduction for a larger number of nodes can be intuitively explained as follows. As demonstrated later (in Section 6.1), K and MK methods tend to overestimate the drone’s duration reduction ability and thus overuse the drone. So, with more nodes, the total time wasted by one vehicle waiting for the other accumulates and amounts to an especially longer tour duration for the K and MK methods, relative to the P method. The P method does not suffer from this problem given its accurate estimate of the drone travel time. As the number of nodes increases, the number of operations grows faster than linearly, and the total tour duration grows slower than

linearly (a well-known result from the TSP literature), together resulting in a higher percentage reduction for the P method compared to the K and MK methods. In practice, this observation implies that as the demand for e-commerce delivery increases, a better estimate of drone travel time brings even greater benefits.

In terms of truck speed, the duration reduction peaks at around 60 km/h compared to the K method, and around 50 km/h compared to the MK method. This suggests that our P method adds the most value at intermediate truck speeds, which can be explained by recognizing the following two opposite factors. On the one hand, at high truck speeds, the usefulness of a drone diminishes regardless of the chosen optimization method, resulting in smaller differences between methods. On the other hand, at low truck speeds, since the drone travels much faster than the truck, the different methods result in a similar set of operations being chosen, lowering the relative benefits of the P method: the large differential between truck and drone speeds implies that the operations favored by the K and MK methods under their overestimation of the drone's ability are also favored under the more realistic drone speed estimates by the P method. The net effect of these two opposite factors amounts to the highest benefits of the P method at intermediate truck speeds.

Overall, the P method consistently outperforms the K and MK methods, with the most impressive benefits in the more practical parameter ranges, namely, at more delivery locations and intermediate truck speeds.

5.1.3. Drone Energy Consumption Reduction: As mentioned in Section 3.2, we use drone energy consumption (DEC) minimization as a secondary objective to break the ties if multiple tours have the same duration. Let γ_i^P , γ_i^K , and γ_i^{MK} , respectively, be the DEC of the solutions obtained for the i^{th} instance using the P, K and MK methods. We calculate the average drone energy savings as $\frac{1}{100} \sum_{i \in \{1, \dots, 100\}} \frac{\gamma_i^K - \gamma_i^P}{\gamma_i^K}$ and $\frac{1}{100} \sum_{i \in \{1, \dots, 100\}} \frac{\gamma_i^{MK} - \gamma_i^P}{\gamma_i^{MK}}$, and report them in Table 8 and Figure 8 (in Appendix A).

The P method reduces the average DEC for all 49 combinations, compared to the K method, and for 40 of the 49 combinations compared to the MK method. On average, the P method produces a 31.61% and 20.01% lower DEC, compared to the K and MK methods, respectively. Similar to the pattern observed for the duration reduction, DEC savings also increase with more nodes, as the inefficient assignment of deliveries to the two vehicles causes more hovering time for the drone waiting for the truck, wasting more drone energy. As expected, under such suboptimal assignments, DEC accumulates faster than linearly with the increasing number of deliveries. Compared to the reduction in tour duration, the DEC savings peak earlier: at 40 km/h compared to K and 30 km/h compared to the MK method, because higher truck speeds undermine the DEC savings more directly than the tour duration savings. Overall, as with the duration reduction, our P method produces substantial DEC reduction, especially with more nodes and low to medium truck speeds.

5.2. Scenario II: With Restricted Airspaces

5.2.1. Benefits of Using a Drone: Table 9 and Figure 9 (in Appendix A) demonstrate the benefits of using a drone in Scenario II. Across 4,900 instances, 4,586 (that is, 93.59%) result in a strict improvement in tour duration. Similar to Scenario I, columns 2-8 in Table 9 show that the duration reduction occurs

Table 9: Comparing the P method with the Truck-only TSP for Scenario II (with RAS). Columns 2-8 list the number of instances (out of 100) where the P method strictly outperforms the Truck-only TSP in terms of the tour duration. Columns 9-15 list the average percentage reduction in duration by the P method compared to Truck-only TSP.

Metrics		Instances Where P Outperforms Truck-only TSP							Avg. Reduction (%) in Duration by P method						
Nodes	Speed (km/h)	20	30	40	50	60	70	80	20	30	40	50	60	70	80
	10		88	85	81	73	67	61	57	14.19	13.98	11.06	7.46	4.02	2.64
20		98	98	96	91	85	82	83	18.57	17.28	14.94	11.55	8.81	7.43	6.22
50		100	100	100	98	95	90	93	18.18	16.43	14.07	10.93	8.45	6.81	6.07
75		100	100	100	100	98	98	96	19.83	17.42	14.81	11.52	8.80	7.30	6.36
100		100	100	100	99	100	98	99	19.79	17.64	14.46	11.11	8.81	6.71	5.59
175		100	100	98	100	100	98	96	18.57	15.61	13.07	10.34	8.30	6.72	5.22
250		100	100	100	97	97	98	93	17.54	14.49	11.57	8.76	6.89	5.85	4.06

Table 10: Comparing the P method with the K and MK methods on total duration for Scenario II (with RAS). Columns 2-8 (respectively, columns 9-15) list the average percentage reduction by the P method compared to the K (respectively, MK) method. Each row shows a different number of nodes and each column a different truck speed.

Metrics		Avg. Reduction (%) in Duration by P vs. K							Avg. Reduction (%) in Duration by P vs. MK						
Nodes	Speed (km/h)	20	30	40	50	60	70	80	20	30	40	50	60	70	80
	10		0.27	0.87	1.67	4.45	6.82	7.24	5.05	0.02	-0.05	-0.47	0.27	-0.43	-0.18
20		0.45	1.74	5.04	8.74	12.88	9.79	6.93	0.20	0.68	1.20	1.69	-0.03	0.07	-0.49
50		1.39	4.87	11.63	18.87	21.34	16.47	12.09	0.92	3.25	7.54	7.40	2.43	1.11	1.23
75		2.34	7.44	16.46	24.11	25.39	18.73	15.34	1.91	6.05	12.07	11.45	3.61	2.64	2.65
100		3.81	11.87	21.40	28.39	29.34	21.66	17.20	3.38	9.63	16.65	15.02	6.16	4.23	4.33
175		8.19	20.11	31.89	37.50	37.58	28.85	24.33	7.72	18.30	26.42	24.82	12.66	10.68	9.63
250		12.89	27.81	38.89	44.32	43.01	33.52	29.13	12.39	25.97	33.85	30.52	17.69	16.44	14.02

Table 11: Comparing the P method with the K and MK methods on DEC for Scenario II (with RAS). Columns 2-8 (respectively, columns 9-15) list the average percentage reduction by the P method compared to the K (respectively, MK) method. Each row shows a different number of nodes and each column a different truck speed.

Metrics		Average reduction (%) in DEC by P vs. K							Average reduction (%) in DEC by P vs. MK						
Nodes	Speed (km/h)	20	30	40	50	60	70	80	20	30	40	50	60	70	80
	10		1.32	2.80	6.10	14.40	21.35	21.47	11.10	-1.15	-0.23	-0.37	3.19	-7.81	-2.70
20		1.80	4.77	11.98	19.15	25.62	22.44	15.99	1.07	2.93	6.69	8.59	-0.12	-3.00	-3.81
50		6.93	16.49	25.27	31.94	33.35	28.23	20.10	6.39	14.65	20.74	19.26	5.73	1.54	1.63
75		11.37	22.70	31.78	37.33	36.59	30.65	23.12	10.72	21.00	27.59	24.78	9.00	5.96	4.70
100		15.92	29.33	38.59	41.70	41.34	32.23	25.24	15.32	27.21	33.77	29.02	14.27	7.46	6.80
175		26.98	40.88	49.32	51.80	49.58	40.35	33.57	26.46	39.36	44.64	39.72	22.46	17.53	14.85
250		34.85	49.09	55.87	58.55	55.89	46.12	39.65	34.46	47.60	51.55	46.81	30.46	26.22	22.07

more frequently at lower truck speeds and more nodes, and columns 9-15 in Table 9 show that the average percentage reduction is also higher at lower truck speeds. However, unlike Scenario I (where columns 9-15 in Table 6 show a higher average percentage reduction at fewer nodes), columns 9-15 in Table 9 show that, with more nodes, the benefit of using the drone first increases and then decreases. This is because at a lower

number of nodes, additional nodes present more chances for the drone to help with the delivery (a much stronger effect than in Scenario I, as shown in columns 2-8 in Table 9 vs. Table 6), which contributes to improving the average benefit of the drone. However, as the number of nodes grows further, the denominator in the percentage reduction becomes larger, resulting in a smaller percentage reduction in duration.

5.2.2. Benefits of Our Solution Approach: Table 10 and Figure 10 (in Appendix A) quantify the average percentage reduction in tour duration achieved by the P method compared to the K and MK methods, in Scenario II. The P method outperforms the K method in all 49 combinations and outperforms the MK method in 43 of the 49 combinations. The average percentage reduction in duration is 16.74% with respect to the K method and 7.90% relative to the MK method, which align closely (and are slightly better) than Scenario I. As with Scenario I, the duration reduction tends to increase as the number of nodes grows, but peaks at intermediate truck speeds of around 50-60 km/h compared to the K method and at around 40-50 km/h compared to the MK method. Overall, we find that, even with the incorporation of RAS, the duration reduction benefits are comparable to those without RAS and exhibit similar broad patterns.

5.2.3. Drone Energy Consumption Reduction: Table 11 and Figure 11 (in Appendix A) present the DEC reduction using the P method compared to the K and MK methods in Scenario II. The average reduction in DEC is 28.43% and 15.79% compared to the K and MK methods—numbers that are similar, albeit slightly lower, than in Scenario I. As the node count increases, the advantage of the P method generally increases. In terms of truck speed, DEC savings also peak around 50-60 km/h compared to the K method and around 40-50 km/h compared to the MK method. In summary, the qualitative and quantitative findings related to the benefits of P method remain largely the same regardless of whether the service area has RAS.

6. Practical Case Studies and Managerial Insights

To demonstrate the effectiveness of our mathematical and computational approach in real-world settings, we conducted case studies in four major US city centers. We directly use the NN predictor trained in Scenario I in Section 5 to run the experiments in this section, demonstrating its robustness across different settings.

We obtained road networks and building locations from the OpenStreetMap NetworkX Python package (OSMNX) (Boeing 2024). For each selected region in the city (5 km \times 5 km, centered on downtown), we identified all buildings and set the probability of having a delivery node at a building to be proportional to the volume of each building. From real-world data in these regions, we observed that the total footprint of all *tall* buildings (taller than the drone’s maximum allowed flying altitude) constituted less than 1% of the total area (5 km \times 5 km). Thus, in these case studies, there are effectively no restricted airspaces. We sampled 200 delivery locations for a typical day, repeating 50 times to ensure statistical robustness and produce average results for each city. We assumed a maximum drone speed of 70 km/h (Federal Aviation Administration 2020) and an average truck speed of 40 km/h (i.e., 25 mi/h), common in busy downtowns. Each truck-and-drone tour plan in our practical case studies was computed in at most 38 seconds of runtime.

For convenient visualization, Section 6.1 uses a smaller (50-node) example from Section 5 to demonstrate the key differences between the truck-and-drone tours generated using our P method and those using the two algorithmic benchmarks (K and MK methods). Then Section 6.2 quantifies the degree to which the P method outperforms the K and MK methods, as well as the truck-only TSP solutions for the real-world case studies described at the beginning of this section. Finally, in Section 6.3, we identify the main attributes of the solutions generated by our approach that drive these improvements for real-world case studies.

6.1. Tour Structure

We now analyze common structures in our truck-and-drone solutions compared to the benchmarks, to understand why we see relative improvements, and to identify the key drivers of improvement explained in Section 6.3. Figure 1 shows the optimal tours obtained using the K, MK, and P methods for a representative example instance with 50 uniformly generated delivery locations without RAS. Black crosses represent drone delivery locations, green dotted lines represent drone trajectories, purple dots represent truck delivery locations, and purple lines represent truck paths. Across the three solutions, the drone typically serves delivery nodes located near the truck path, on either side, but requires inconvenient detours to the truck path to serve these nodes via truck. In such cases, drone deliveries are more efficient by avoiding such detours.

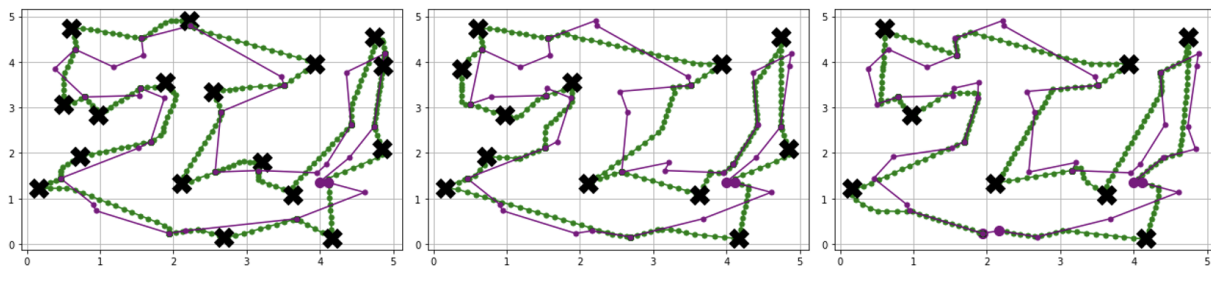


Figure 1: Example tour solutions using K (left), MK (middle) and P (right) methods with the same instance.

We observe that in the K and MK solutions, which assume Euclidean and modified Euclidean drone travel, the drone’s effectiveness in reducing the tour duration is overestimated, resulting in more drone nodes (17 and 12 in this example), compared to the solution from the P method (which has eight nodes here). Moreover, the drone nodes selected in the P solution are often subsets of the drone nodes in the K and MK solutions. These patterns are broadly seen beyond this illustrative example, which motivates Section 6.3.

6.2. Benefits of Optimization

In this section, we quantify the degree of improvement achieved by the P, K, and MK methods, compared to the truck-only TSP solution, and also the improvement achieved by the P method compared to the K and MK methods. We consider two different assumptions about truck travel: straight-line Euclidean travel (an assumption used in most of the existing literature, ensuring easier comparison) and travel along the actual road network (a more realistic assumption, ensuring more practicality). Tables 12 and 13 and Figure 2

Table 12: Case studies using straight-line distances for truck travel (T stands for the Truck-only TSP tour).

Metric	Stat	Boston	Chicago	Philadelphia	Los Angeles	Average
K vs. T duration	Mean	-89.24%	-82.75%	-37.56%	-29.05%	-59.65%
	95% CI	[-92.02%, -86.47%]	[-85.18%, -80.32%]	[-39.47%, -35.65%]	[-30.93%, -27.17%]	[-61.90%, -57.40%]
	Count	0	0	0	0	0
MK vs. T duration	Mean	-72.42%	-63.29%	-27.25%	-20.21%	-45.79%
	95% CI	[-75.34%, -69.51%]	[-66.06%, -60.51%]	[-29.09%, -25.41%]	[-22.11%, -18.31%]	[-48.15%, -43.43%]
	Count	0	0	0	0	0
P vs. T duration	Mean	9.87%	10.64%	7.53%	7.67%	8.93%
	95% CI	[8.13%, 11.61%]	[8.89%, 12.40%]	[6.28%, 8.77%]	[6.38%, 8.96%]	[7.42%, 10.43%]
	Count	47	46	48	46	46.75
P vs. K duration	Mean	52.31%	51.02%	32.64%	28.28%	41.06%
	95% CI	[51.42%, 53.21%]	[49.93%, 52.11%]	[31.49%, 33.80%]	[26.92%, 29.64%]	[39.94%, 42.19%]
	Count	50	50	50	50	50
P vs. MK duration	Mean	47.64%	45.16%	27.19%	22.92%	35.73%
	95% CI	[46.69%, 48.60%]	[44.02%, 46.29%]	[26.00%, 28.38%]	[21.18%, 24.66%]	[34.47%, 36.98%]
	Count	50	50	50	50	50
P vs. K DEC	Mean	71.56%	70.37%	60.05%	56.19%	64.54%
	95% CI	[71.09%, 72.03%]	[69.86%, 70.89%]	[59.49%, 60.60%]	[55.59%, 56.79%]	[64.01%, 65.08%]
	Count	50	50	50	50	50
P vs. MK DEC	Mean	68.49%	66.58%	55.90%	52.04%	60.75%
	95% CI	[67.81%, 69.17%]	[65.86%, 67.30%]	[55.21%, 56.58%]	[51.34%, 52.74%]	[60.05%, 61.45%]
	Count	50	50	50	50	50

Table 13: Case studies using road network-based distances for truck travel (T stands for the Truck-only TSP tour).

Metric	Stat	Boston	Chicago	Philadelphia	Los Angeles	Average
K vs. T duration	Mean	26.46%	24.44%	18.58%	14.12%	20.90%
	95% CI	[25.56%, 27.37%]	[23.47%, 25.42%]	[17.70%, 19.47%]	[13.00%, 15.25%]	[19.93%, 21.88%]
	Count	50	50	50	50	50
MK vs. T duration	Mean	27.12%	25.13%	19.02%	14.65%	21.48%
	95% CI	[26.17%, 28.07%]	[24.20%, 26.05%]	[18.13%, 19.92%]	[13.57%, 15.72%]	[20.52%, 22.44%]
	Count	50	50	50	50	50
P vs. T duration	Mean	28.48%	26.25%	20.27%	17.26%	23.06%
	95% CI	[27.63%, 29.33%]	[25.39%, 27.12%]	[19.39%, 21.14%]	[16.38%, 18.13%]	[22.20%, 23.93%]
	Count	50	50	50	50	50
P vs. K duration	Mean	2.70%	2.31%	2.02%	3.52%	2.64%
	95% CI	[1.92%, 3.48%]	[1.31%, 3.32%]	[1.19%, 2.85%]	[2.33%, 4.71%]	[1.69%, 3.59%]
	Count	39	38	40	41	39.5
P vs. MK duration	Mean	1.81%	1.43%	1.49%	2.94%	1.92%
	95% CI	[1.10%, 2.53%]	[0.45%, 2.42%]	[0.71%, 2.28%]	[1.77%, 4.11%]	[1.00%, 2.84%]
	Count	38	33	40	38	37.25
P vs. K DEC	Mean	14.02%	17.88%	13.92%	21.20%	16.76%
	95% CI	[13.16%, 14.88%]	[16.88%, 18.88%]	[13.06%, 14.78%]	[19.89%, 22.51%]	[15.75%, 17.76%]
	Count	50	50	50	50	50
P vs. MK DEC	Mean	12.75%	16.64%	13.16%	20.60%	15.78%
	95% CI	[11.80%, 13.69%]	[15.70%, 17.58%]	[12.29%, 14.02%]	[19.28%, 21.92%]	[14.77%, 16.80%]
	Count	50	50	50	50	50

summarize the improvements in terms of tour duration (in the first five main rows of the tables) and DEC (in the last two main rows). Each main row presents the mean and the 95% confidence interval of the percentage improvement, as well as the count of how many of the 50 instances show a positive improvement.

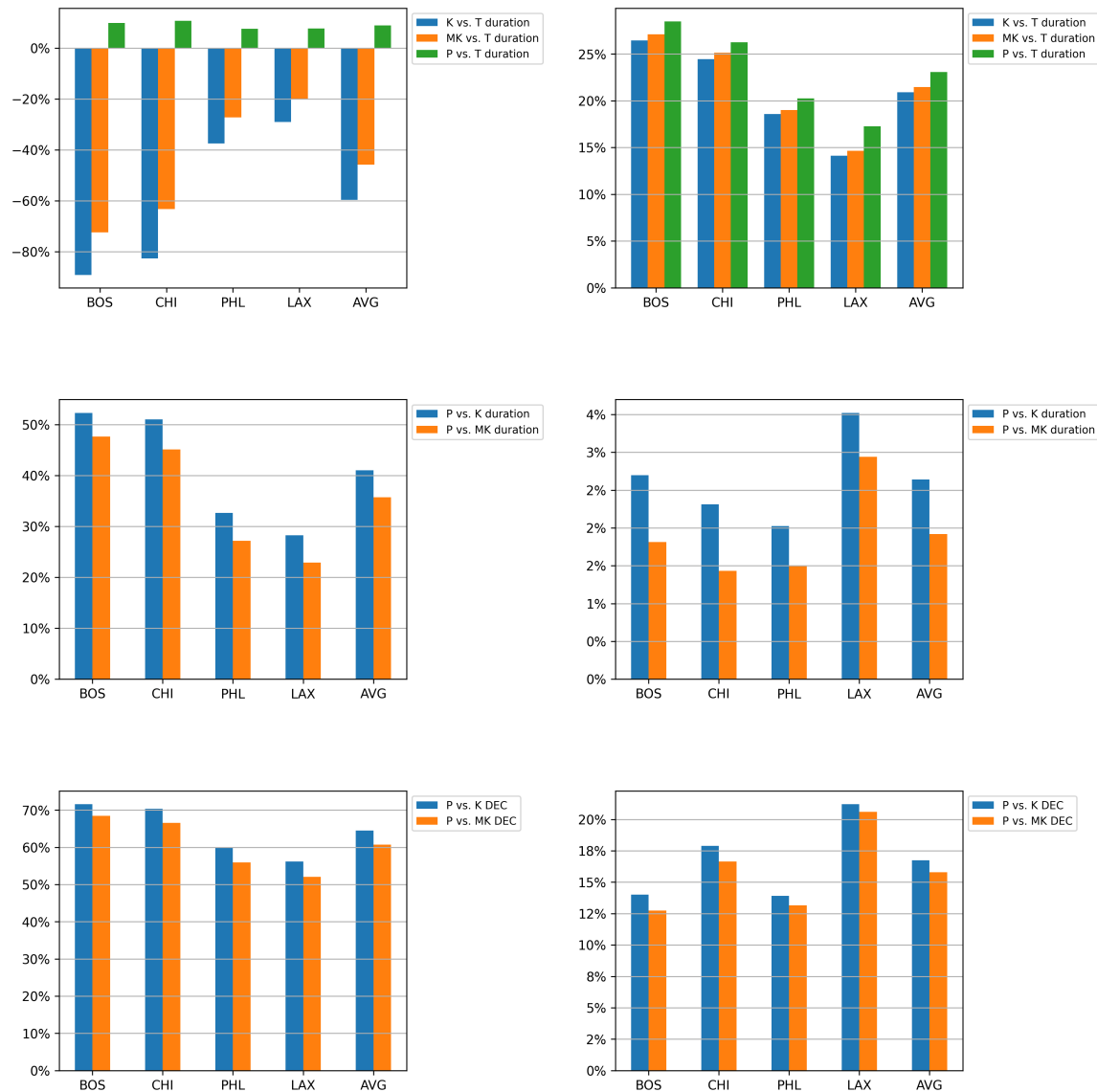


Figure 2: Case study results assuming straight-line (left) and road network-based (right) truck travels.

Across four cities and both truck travel assumptions, our P method always performs the best in terms of both tour duration and DEC. Depending on the specific structures of the demand distributions and road networks in each downtown area, the actual duration reduction and the DEC savings vary. Across four cities and two truck travel assumptions, the P method reduces tour duration by 2.02%-52.31% compared to the K method and by 1.43%-47.64% compared to the MK method. In addition, the P method reduces DEC by 13.92%-71.56% compared to the K method and by 12.75%-68.49% compared to the MK method. P method also outperforms the T method (that is, the truck-only TSP tour) by 7.53%-28.48% in terms of the tour duration, across the four cities and two truck travel assumptions. Under road network-based truck travel, the K and MK methods also outperform truck-only tour by 14.12%-27.12% demonstrating that, in this case, the drone adds value regardless of the optimization method used in truck-and-drone tour planning. However,

as shown in Table 12, under the straight-line Euclidean truck travel assumption, the tour duration actually worsens significantly for the K and MK methods compared to the T method. This highlights the fact that, in some cases, inaccurate estimates of drone travel times can completely nullify the benefits of a drone.

Although Table 13 shows a smaller improvement achieved by the P method compared to the K, MK and T methods than in Table 12, the 95% confidence intervals demonstrate that all improvements are statistically significant. Moreover, these improvements are also practically very significant, from the point of view of the e-commerce companies. Amazon delivers more than 10 million customer packages per day (Yaqub 2025), and each driver makes 180 stops and delivers 250-300 packages a day (Capital One Shopping Research Team 2024), which corresponds to more than 33,333 truck drivers in service each day. Assuming a total cost of operation for a truck of \$90.78/hour (Fisher 2023), the resulting 1.92% average reduction in duration using the P method, even compared to the better of the two benchmarks (the MK method) and even under the assumption of road network-based truck travel, translates into daily savings of more than \$200,000.

In summary, we find that our P method consistently and substantially outperforms all benchmarks under all tested assumptions, providing significant benefits both from a statistical and a practical standpoint.

6.3. Drivers of Improvement

We further analyze the results of case studies in which the truck travels along the road network in the downtown areas of Boston (BOS), Philadelphia (PHL), Chicago (CHI), and Los Angeles (LAX), to identify three main drivers of the improvement achieved by our P method compared to the benchmarks. These drivers include more truck delivery nodes, judicious reconfiguration of drone operations to retain most high-quality drone nodes, and large drone travel savings at the expense of small increases in truck travel distances.

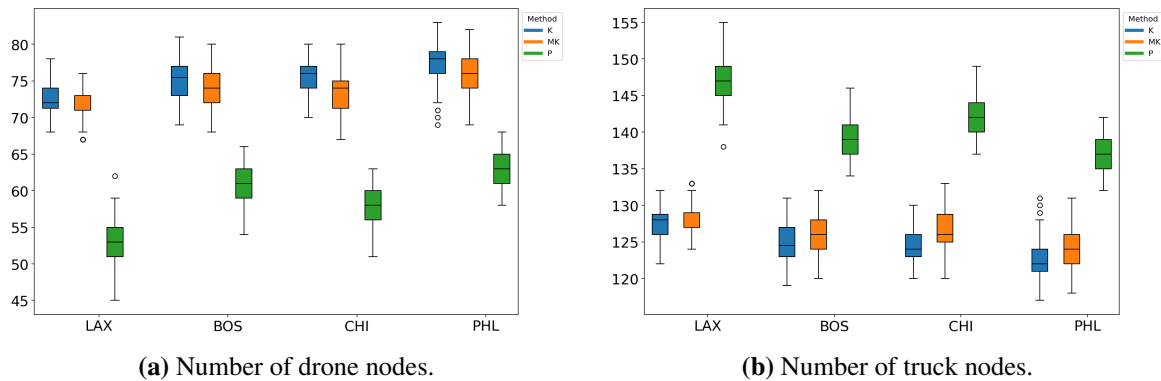
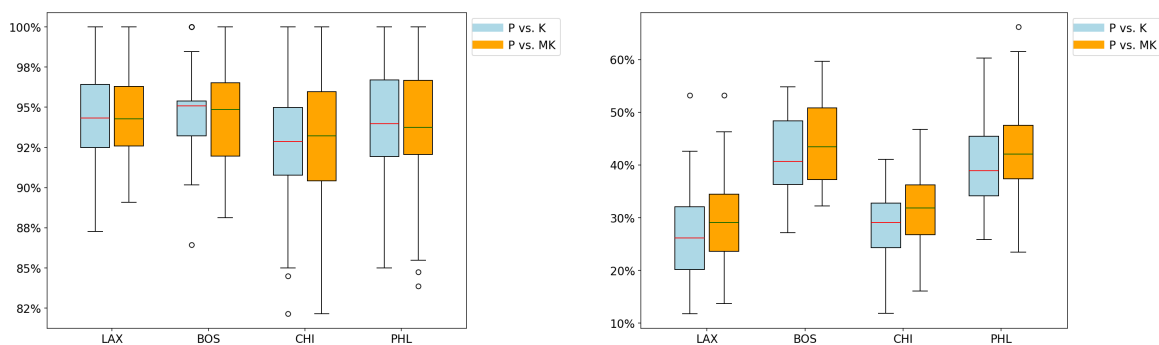


Figure 3: Number of drone nodes (left) and truck nodes (right) averaged across the 50 instances.

More truck delivery nodes: The K method, used extensively by previous studies in truck-and-drone tour planning, assumes Euclidean travel distances for the drone, while the MK method, developed by us, partially alleviates this shortcoming using a multiplier to adjust the drone travel time. Because of their reliance on Euclidean distances, we found that both K and MK methods tend to overestimate the drone’s ability for fast

deliveries. They both tend to use more drone operations than the P method, end up making the truck wait long periods for the drone to return, and thus increase the tour duration. Figure 3 quantifies this effect by plotting the number of nodes served by the drone (in the left sub-figure) and the truck (in the right sub-figure) for each of the four cities and the three methods, namely K, MK and P. Figure 3 shows that, across the four cities, the P method reduces the number of drone nodes by 21.7% and 20.3%, resulting in 13.0% and 11.8% more truck delivery nodes for the P method, compared to the K and MK methods, respectively. This overuse of drone nodes degrades the performance of the K and MK methods, and avoiding this pitfall in turn is an important driver of the superior performance of the P method.



(a) Percentage of P method's drone nodes that are drone nodes in the benchmark method.

(b) Percentage of P method's drone operations that are drone operations in the benchmark method.

Figure 4: Percentage of P method's drone nodes and drone operations that overlap with those in benchmarks.

Judicious reconfiguration of drone operations to retain high-quality drone nodes: In addition to avoiding overreliance on drone operations, the P method succeeds in retaining almost all high-quality drone nodes. Figure 4a shows the number of drone nodes in the P method's solution that are also assigned to the drone in a benchmark method (K and MK) as a percentage of the total number of drone nodes in the P method's solution. The right sub-figure analogously shows the same metrics, but for drone operations rather than drone nodes, where a drone operation is defined as a 3-tuple consisting of the operation start node, drone node, and operation end node. Across all 200 instances in the four cities, 94% of the drone nodes in the P method's solution are also found to be drone nodes in each of the K and MK methods' solutions.

However, a very different picture emerges in terms of overlaps in drone operations across different methods, as seen in Figure 4b. Across all instances in the four cities, only 34.3% and 37.2% of the drone operations in the P method's solution are in the solutions of the K and MK methods, respectively. The contrast is even more striking if we focus on matching the entire operation, i.e., matching operation start node, operation end node, drone node and the entire sequence of truck-only nodes in an operation. Across the 200 instances in these four cities, *none* of the operations chosen by the P method completely matches any of those chosen by either of the benchmarks (K or MK). Overall, across the 200 instances, although

almost all ($\sim 94\%$) of the drone nodes selected by the P method are those in the benchmarks, only a third (34.3%-37.2%) of the drone operations match those in the benchmark solutions, and none of the operations match entirely. This suggests that the P method judiciously reconfigures the drone operations by changing the operation start/end nodes and truck visit sequence to generate more efficient operations, without relinquishing the high-quality drone nodes, which is a major driver of improvement obtained by the P method.

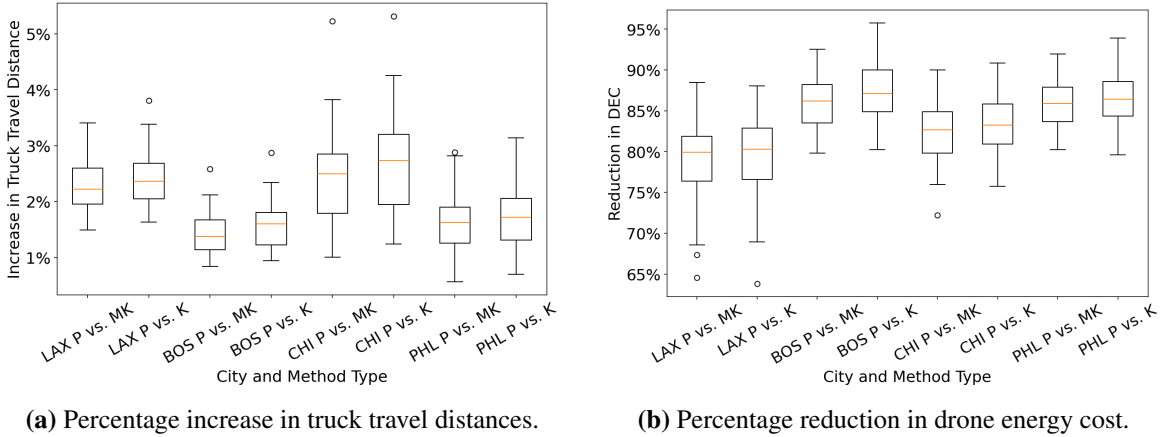


Figure 5: Increase in truck travel distance and DEC savings achieved by the P method relative to the benchmarks.

Large drone travel savings at the expense of small increases in truck travel distances: A third key driver of improvement is the ability of the P method’s solutions to achieve large reductions in drone travel in exchange of slight increases in truck travel. Figure 5 shows that, compared to the K and MK methods, the P method increases the total distance traveled by the truck by only 2.1% and 1.9% of the the truck-only TSP length, but significantly reduces the drone energy consumption by 16.8% and 15.8%, respectively.

7. Conclusion

We formulate a nonlinear, multi-objective, truck-and-drone model that integrates drone flight physics within the combinatorial complexity of the truck routing problem. We propose a new end-to-end solution method that combines optimization and machine learning to improve solution quality while solving the tour optimization problem in 1-3 minutes. Our results from a series of computational experiments and practical case studies demonstrate consistent and substantial improvements over state-of-the-art approaches that neglect drone-flight physics. This underscores the importance of integrating accurate drone trajectory modeling into delivery planning systems to realize the full potential of truck-and-drone collaborative logistics, resulting in annual savings worth millions of dollars, while also benefiting the environment.

Future research could extend our approach in many promising directions. One can incorporate additional practical considerations for both truck and drone—such as, variations in wind conditions, which requires adding an extra constraint in the drone model. Extending to other system configurations—for example,

adding multiple drones or increasing the number of drone flights from and to the same nodes—could enhance operational flexibility. Lastly, while we focus on drone energy savings only as a secondary objective, a more holistic approach to studying the energy costs of electric trucks and advanced battery-powered drones may yield valuable insights into the overall environmental benefits and carbon reduction strategies.

References

- Adbelhafiz M, Mostafa A, Girard A (2010) Vehicle routing problem instances: Application to multi-UAV mission planning. *AIAA Guidance, Navigation, and Control Conference*, 8435.
- Agatz N, Bouman P, Schmidt M (2018) Optimization approaches for the traveling salesman problem with drone. *Transportation Science* 52(4):965–981.
- Amorosi L, Puerto J, Valverde C (2021) Coordinating drones with mothership vehicles: The mothership and drone routing problem with graphs. *Computers & Operations Research* 136:105445.
- Applegate DL (2006) *The traveling salesman problem: a computational study*, volume 17 (Princeton university press).
- Ayranci ZB (2016) Use of drones in sports broadcasting. *Ent. & Sports Law*. 33:79.
- Bengio Y (2012) Practical recommendations for gradient-based training of deep architectures. *Neural networks: Tricks of the trade: Second edition*, 437–478 (Springer).
- Bengio Y, Lodi A, Prouvost A (2021) Machine learning for combinatorial optimization: a methodological tour d’horizon. *European Journal of Operational Research* 290(2):405–421.
- Boeing G (2024) Modeling and analyzing urban networks and amenities with osmnx. *en. In:()* .
- Borrelli F, Subramanian D, Raghunathan AU, Biegler LT (2006) MILP and NLP techniques for centralized trajectory planning of multiple unmanned air vehicles. *2006 American Control Conference (IEEE)*.
- Bottou L, Curtis FE, Nocedal J (2018) Optimization methods for large-scale machine learning. *SIAM review* 60(2):223–311.
- Bouman P, Agatz N, Schmidt M (2018) Dynamic programming approaches for the traveling salesman problem with drone. *Networks* 72(4):528–542.
- Capital One Shopping Research Team (2024) Amazon logistics statistics (2024): Number of package deliveries. URL <https://capitaloneshopping.com/research/amazon-logistics-statistics/>.
- Chaudhuri D, Murthy C, Chaudhuri B (1992) A modified metric to compute distance. *Pattern Recognition* 25(7):667–677.
- Choi Y, Schonfeld PM (2021) A comparison of optimized deliveries by drone and truck. *Transportation Planning and Technology* 44(3):319–336.
- Chung SH, Sah B, Lee J (2020) Optimization for drone and drone-truck combined operations: A review of the state of the art and future directions. *Computers & Operations Research* 123:105004.
- Croes GA (1958) A method for solving traveling-salesman problems. *Operations Research* 6(6):791–812.

- Das DN, Sewani R, Wang J, Tiwari MK (2020) Synchronized truck and drone routing in package delivery logistics. *IEEE Transactions on Intelligent Transportation Systems* 22(9):5772–5782.
- de Freitas JC, Penna PHV (2020) A variable neighborhood search for flying sidekick traveling salesman problem. *International Transactions in Operational Research* 27(1):267–290.
- de Freitas JC, Penna PHV, Toffolo TA (2023) Exact and heuristic approaches to truck–drone delivery problems. *EURO Journal on Transportation and Logistics* 12:100094.
- Federal Aviation Administration (2020) Small unmanned aircraft systems (UAS) regulations - part 107. URL <https://www.faa.gov/newsroom/small-unmanned-aircraft-systems-uas-regulations-part-107>.
- Fisher T (2023) Cost of operating a truck reaches all-time high. URL <https://landline.media/cost-of-operating-a-truck-reaches-all-time-high/>.
- Fügenschuh A, Müllenstedt D, Schmidt J (2021) Flight planning for unmanned aerial vehicles. *Military Operations Research* 26(3):49–71.
- Gao J, Zhen L, Laporte G, He X (2023) Scheduling trucks and drones for cooperative deliveries. *Transportation Research Part E: Logistics and Transportation Review* 178:103267.
- Garg V, Niranjana S, Prybutok V, Pohlen T, Gligor D (2023) Drones in last-mile delivery: A systematic review on efficiency, accessibility, and sustainability. *Transportation Research Part D: Transport and Environment* 123:103831.
- Gasse M, Chételat D, Ferroni N, Charlin L, Lodi A (2019) Exact combinatorial optimization with graph convolutional neural networks. *Advances in neural information processing systems* 32.
- Geiger B, Horn J, DeLullo A, Niessner A, Long L (2006) Optimal path planning of UAVs using direct collocation with nonlinear programming. *AIAA Guidance, Navigation, and Control Conference and Exhibit*, 6199.
- Glorot X, Bordes A, Bengio Y (2011) Deep sparse rectifier neural networks. *Proceedings of the fourteenth international conference on artificial intelligence and statistics*, 315–323 (JMLR Workshop and Conference Proceedings).
- Goodfellow I, Bengio Y, Courville A, Bengio Y (2016) *Deep learning*, volume 1 (MIT press Cambridge).
- Ha QM, Deville Y, Pham QD, Hà MH (2018) On the min-cost traveling salesman problem with drone. *Transportation Research Part C: Emerging Technologies* 86:597–621.
- Helsgaun K (2000) An effective implementation of the lin–kernighan traveling salesman heuristic. *European journal of operational research* 126(1):106–130.
- Hizir AE, Barnhart C, Vaze V (2025) Large-scale airline crew recovery using mixed-integer optimization and supervised machine learning. Available at SSRN 5180044 .
- Hornik K, Stinchcombe M, White H (1989) Multilayer feedforward networks are universal approximators. *Neural networks* 2(5):359–366.

- Jeong HY, David JY, Min BC, Lee S (2020) The humanitarian flying warehouse. *Transportation research part E: logistics and transportation review* 136:101901.
- Jeong HY, Lee S (2023) Drone routing problem with truck: Optimization and quantitative analysis. *Expert Systems with Applications* 227:120260.
- Jun M, D'Andrea R (2003) Path planning for unmanned aerial vehicles in uncertain and adversarial environments. *Cooperative control: models, applications and algorithms* 95–110.
- Khalil EB, Dilkina B, Nemhauser GL, Ahmed S, Shao Y (2017) Learning to run heuristics in tree search. *Ijcai*, 659–666.
- Kingma DP, Ba J (2014) Adam: A method for stochastic optimization. *arXiv preprint arXiv:1412.6980*.
- Kitjacharoenchai P, Min BC, Lee S (2020) Two echelon vehicle routing problem with drones in last mile delivery. *International Journal of Production Economics* 225:107598.
- Kitjacharoenchai P, Ventresca M, Moshref-Javadi M, Lee S, Tanchoco JM, Brunese PA (2019) Multiple traveling salesman problem with drones: Mathematical model and heuristic approach. *Computers & Industrial Engineering* 129:14–30.
- Kloster K, Moeini M, Vigo D, Wendt O (2023) The multiple traveling salesman problem in presence of drone-and robot-supported packet stations. *European Journal of Operational Research* 305(2):630–643.
- Kundu A (2022) *Developing efficient order and split heuristics for coordinated covering tour problems with drones*. Ph.D. thesis, Texas Tech University.
- Kundu A, Escobar RG, Matis TI (2022) An efficient routing heuristic for a drone-assisted delivery problem. *IMA Journal of Management Mathematics* 33(4):583–601.
- Ładyżyńska-Kozdraś E (2012) Modeling and numerical simulation of unmanned aircraft vehicle restricted by non-holonomic constraints. *Journal of Theoretical and Applied Mechanics* 50(1):251–268.
- Larsen E, Lachapelle S, Bengio Y, Frejinger E, Lacoste-Julien S, Lodi A (2018) Predicting solution summaries to integer linear programs under imperfect information with machine learning. *preprint arXiv:1807.11876* 2(4):14.
- LeCun Y, Bottou L, Orr GB, Müller KR (2002) Efficient backprop. *Neural networks: Tricks of the trade*, 9–50 (Springer).
- Leon-Blanco JM, Gonzalez-R PL, Andrade-Pineda JL, Canca D, Calle M (2022) A multi-agent approach to the truck multi-drone routing problem. *Expert Systems with Applications* 195:116604.
- Li H, Chen J, Wang F, Zhao Y (2022) Truck and drone routing problem with synchronization on arcs. *Naval Research Logistics (NRL)* 69(6):884–901.
- Lin M, Chen Y, Han R, Chen Y (2022) Discrete optimization on truck-drone collaborative transportation system for delivering medical resources. *Discrete Dynamics in Nature and Society* 2022(1):1811288.
- Liu Y, Luo Z, Liu Z, Shi J, Cheng G (2019) Cooperative routing problem for ground vehicle and unmanned aerial vehicle: The application on intelligence, surveillance, and reconnaissance missions. *IEEE Access* 7:63504–63518.

- Luo Z, Gu R, Poon M, Liu Z, Lim A (2022) A last-mile drone-assisted one-to-one pickup and delivery problem with multi-visit drone trips. *Computers & Operations Research* 148:106015.
- Luo Z, Poon M, Zhang Z, Liu Z, Lim A (2021) The multi-visit traveling salesman problem with multi-drones. *Transportation Research Part C: Emerging Technologies* 128:103172.
- Macrina G, Pugliese LDP, Guerriero F, Laporte G (2020) Drone-aided routing: A literature review. *Transportation Research Part C: Emerging Technologies* 120:102762.
- Madani B, Ndiaye M (2022) Hybrid truck-drone delivery systems: A systematic literature review. *IEEE Access* 10:92854–92878.
- Marcos Alvarez A, Louveaux Q, Wehenkel L (2014) A supervised machine learning approach to variable branching in branch-and-bound. *Liege University* .
- Marinelli M, Caggiani L, Ottomanelli M, Dell’Orco M (2018) En route truck–drone parcel delivery for optimal vehicle routing strategies. *IET Intelligent Transport Systems* 12(4):253–261.
- Masmoudi MA, Mancini S, Baldacci R, Kuo YH (2022) Vehicle routing problems with drones equipped with multi-package payload compartments. *Transportation Research Part E: Logistics and Transportation Review* 164:102757.
- Moshref-Javadi M, Hemmati A, Winkenbach M (2021) A comparative analysis of synchronized truck-and-drone delivery models. *Computers & Industrial Engineering* 162:107648.
- Moshref-Javadi M, Lee S, Winkenbach M (2020) Design and evaluation of a multi-trip delivery model with truck and drones. *Transportation Research Part E: Logistics and Transportation Review* 136:101887.
- Moshref-Javadi M, Winkenbach M (2021) Applications and research avenues for drone-based models in logistics: A classification and review. *Expert Systems with Applications* 177:114854.
- Murray CC, Chu AG (2015) The flying sidekick traveling salesman problem: Optimization of drone-assisted parcel delivery. *Transportation Research Part C: Emerging Technologies* 54:86–109.
- Murray CC, Raj R (2020) The multiple flying sidekicks traveling salesman problem: Parcel delivery with multiple drones. *Transportation Research Part C: Emerging Technologies* 110:368–398.
- Pasha J, Elmi Z, Purkayastha S, Fathollahi-Fard AM, Ge YE, Lau YY, Dulebenets MA (2022) The drone scheduling problem: A systematic state-of-the-art review. *IEEE Transactions on Intelligent Transportation Systems* 23(9):14224–14247.
- Pohl AJ, Lamont GB (2008) Multi-objective UAV mission planning using evolutionary computation. *2008 winter simulation conference*, 1268–1279 (IEEE).
- Poikonen S, Golden B (2020) The mothership and drone routing problem. *INFORMS Journal on Computing* 32(2):249–262.
- Raj R, Murray C (2020) The multiple flying sidekicks traveling salesman problem with variable drone speeds. *Transportation Research Part C: Emerging Technologies* 120:102813.

- Rashedi N, Sankey N, Vaze V, Wei K (2025) A machine learning approach for solution space reduction in aircraft disruption recovery. *European Journal of Operational Research* 323(1):297–308.
- Rave A, Fontaine P, Kuhn H (2023) Drone location and vehicle fleet planning with trucks and aerial drones. *European Journal of Operational Research* 308(1):113–130.
- Reiter R, Quirynen R, Diehl M, Di Cairano S (2024) Equivariant deep learning of mixed-integer optimal control solutions for vehicle decision making and motion planning. *IEEE Transactions on Control Systems Technology*.
- Remer B, Malikopoulos AA (2019) The multi-objective dynamic traveling salesman problem: Last mile delivery with unmanned aerial vehicles assistance. *2019 American Control Conference (ACC)*, 5304–5309 (IEEE).
- Rhodes F (1995) On the metrics of chauthuri, murthy and chauthuri. *Pattern Recognition* 28(5):745–752.
- Roberti R, Ruthmair M (2021) Exact methods for the traveling salesman problem with drone. *Transportation Science* 55(2):315–335.
- Salama MR, Srinivas S (2022) Collaborative truck multi-drone routing and scheduling problem: Package delivery with flexible launch and recovery sites. *Transportation Research Part E: Logistics and Transportation Review* 164:102788.
- Schmidt J, Fügenschuh A (2023) A two-time-level model for mission and flight planning of an inhomogeneous fleet of unmanned aerial vehicles. *Computational Optimization and Applications* 85(1):293–335.
- Sorbelli FB, Corò F, Palazzetti L, Pinotti CM, Rigoni G (2023) How the wind can be leveraged for saving energy in a truck-drone delivery system. *IEEE Transactions on Intelligent Transportation Systems* 24(4):4038–4049.
- Thomas T, Srinivas S, Rajendran C (2023) Collaborative truck multi-drone delivery system considering drone scheduling and en route operations. *Annals of Operations Research* 1–47.
- US Census Bureau (2025) Quarterly retail e-commerce sales. URL <https://www.census.gov/retail/ecommerce.html>.
- Wang Y, Wang Z, Hu X, Xue G, Guan X (2022) Truck–drone hybrid routing problem with time-dependent road travel time. *Transportation Research Part C: Emerging Technologies* 144:103901.
- Yang Y, Yan C, Cao Y, Roberti R (2023) Planning robust drone-truck delivery routes under road traffic uncertainty. *European Journal of Operational Research* 309(3):1145–1160.
- Yaqub M (2025) 19+ amazon logistics statistics: A must know in 2025. URL <https://www.contimod.com/amazon-logistics-statistics/>.
- Yu S, Puchinger J, Sun S (2024) Electric van-based robot deliveries with en-route charging. *European Journal of Operational Research* 317(3):806–826.
- Zeng F, Chen Z, Clarke JP, Goldsman D (2022) Nested vehicle routing problem: Optimizing drone-truck surveillance operations. *Transportation Research Part C: Emerging Technologies* 139:103645.
- Zhang C, Bengio S, Hardt M, Recht B, Vinyals O (2017) Understanding deep learning requires rethinking generalization. *International Conference on Learning Representations*.

Appendix A: Supplemental Figures for the Computational Results

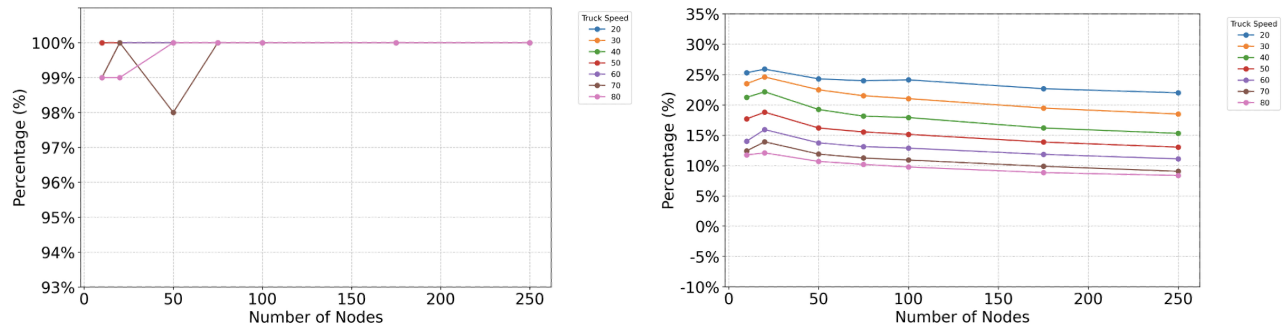


Figure 6: Duration reduction: truck-and-drone tour (P method) vs. Truck-only TSP for Scenario I (without RAS). The left sub-figure shows the percentage of instances for which the P method strictly improves upon the Truck-only TSP duration. The right sub-figure shows the average percentage reduction achieved by the P method compared with the Truck-only TSP.

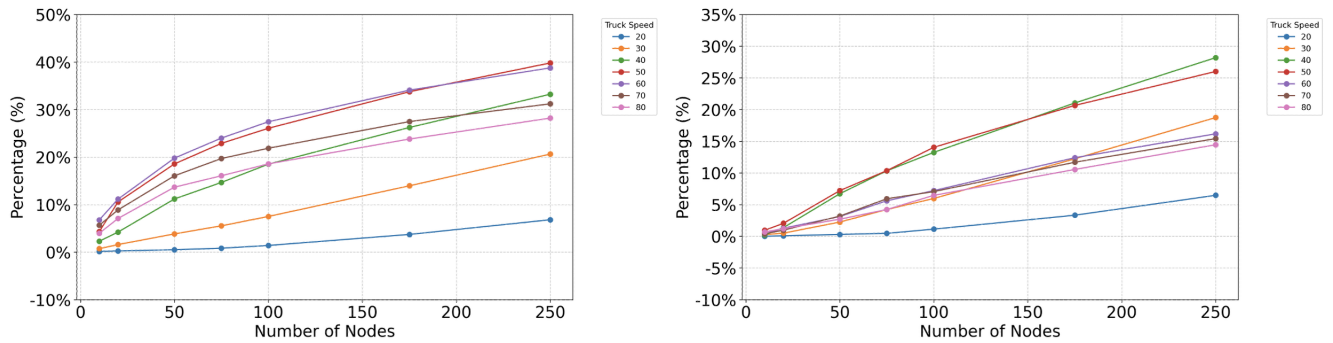


Figure 7: Average percentage reduction in the total tour duration achieved by the P method compared to the K method (left sub-figure) and MK method (right sub-figure) for Scenario I (without RAS).

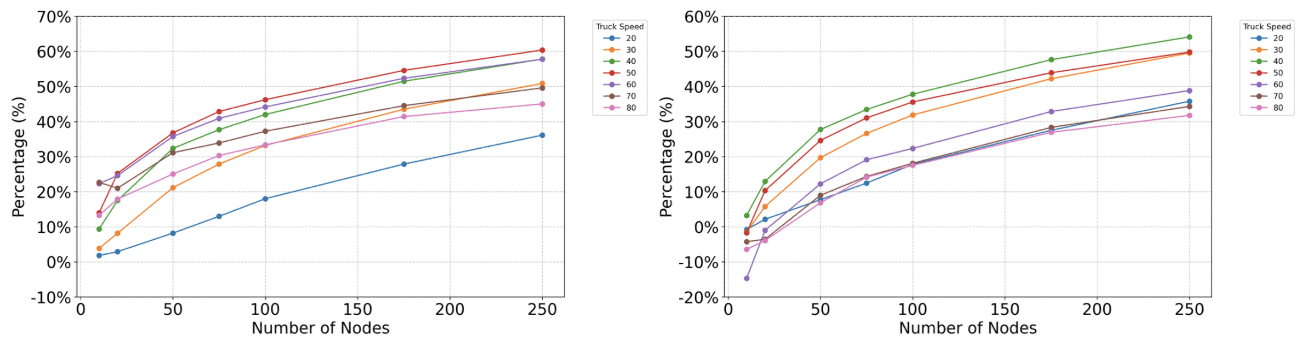


Figure 8: Average percentage reduction in drone energy consumption achieved by the P method compared to the K method (left sub-figure) and MK method (right sub-figure) for Scenario I (without RAS).

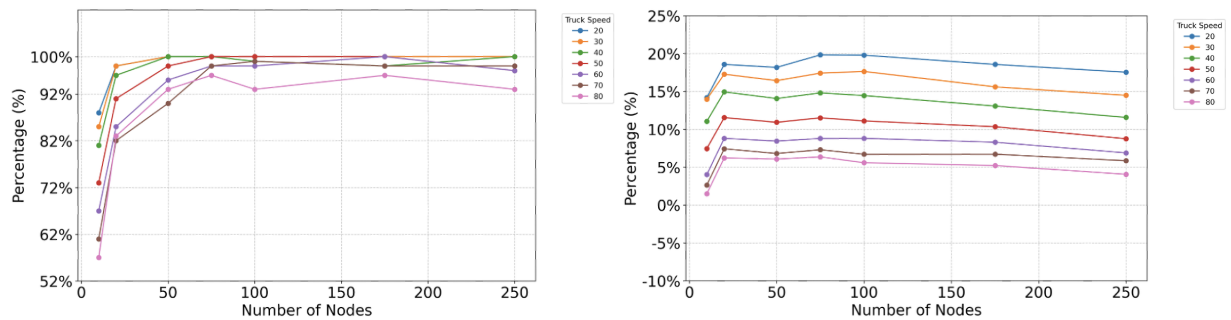


Figure 9: Duration reduction: truck-and-drone tour (P method) vs. Truck-only TSP for Scenario II (with RAS). The left sub-figure shows the percentage of instances for which the P method strictly improves upon the Truck-only TSP duration. The right sub-figure shows the average percentage reduction achieved by the P method compared with the Truck-only TSP.

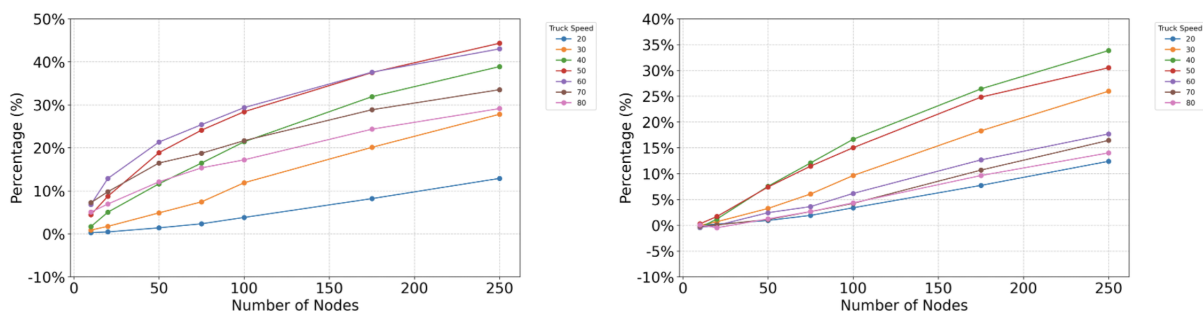


Figure 10: Average percentage reduction in the total tour duration achieved by the P method compared to the K method (left sub-figure) and MK method (right sub-figure) for Scenario II (with RAS).

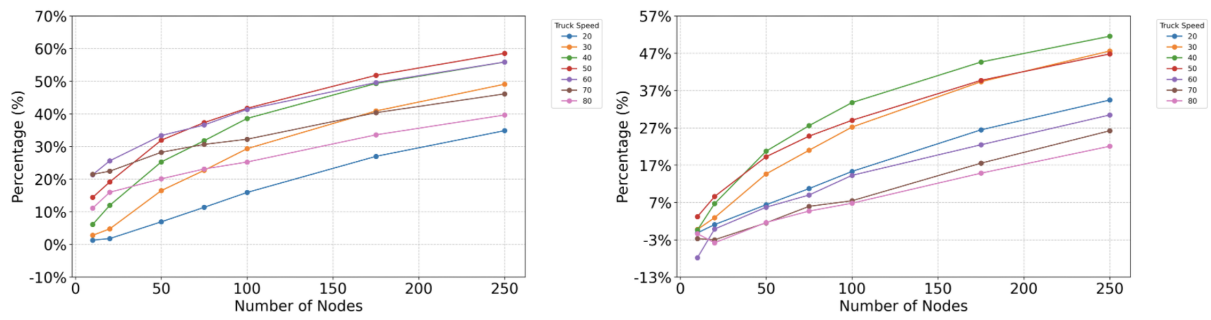


Figure 11: Average percentage reduction in drone energy consumption achieved by the P method compared to the K method (left sub-figure) and MK method (right sub-figure) for Scenario II (with RAS).